PILOT SCALE OPERATION AND TESTING OF SYNGAS CHEMICAL LOOPING FOR HYDROGEN PRODUCTION

FINAL REPORT

AWARDED UNDER

DOE/NETL DE-FE0023915

PREPARED BY

The Ohio State University

151 West Woodruff Ave

Columbus, OH 43210

PRINCIPAL INVESTIGATOR

Professor Liang-Shih Fan

Phone: 614-688-3262

Fax: 614-292-3769

Fan.1@osu.edu

AUTHORS

Tien-Lin Hsieh, Andrew S. Tong, Dikai Xu, Sourabh Nadgouda, Yitao Zhang, Dawei Wang, Cheng L. Chung, Yaswanth Pottimurthy, Mengqing Guo, Liang Zeng, Samuel Bayham, Omar McGiveron, Yu-Yen Chen, Mingyuan Xu, Pengfei He, Liang-Shih Fan

SUBMITTED TO

National Energy Technology Laboratory, Department of Energy

Report Abstract

The Syngas Chemical looping (SCL) process provides efficient and economic means to utilize the abundant fossil reserve of coal. The main problem associated with coal utilization is the CO_2 emissions resulting from its combustion. Even though CO_2 regulation or carbon tax is currently not in place, its enforcement is expected in the near future. Such a greenhouse gas emission control, if adopted in current power plant systems, will drive the efficiency down and increase the cost of electricity, due to the energy and capital-intensive nature of current CO_2 separation techniques. This highlights the need to develop technologies that present a solution to the rising cost of electricity in the future.

The integrated gasification combined cycle (IGCC) presents an improvement to the above predicament, but it is capital intensive due to the extensive unit operations involved. The efficiency for a CO_2 capture incorporated IGCC system is around ~32%, resulting in approximately 45% increase in cost of electricity. This is definitely a better path to traverse than the conventional pulverized coal (PC) power plants as it has improved economics and efficiencies accompanied by product flexibility.

The SCL process advances the benefits even further when integrated with the IGCC process. The SCL process removes the expensive WGS system and CO_2 separation columns, thereby saving on capital and operational expenses. This integration results in a 12 – 21% increase in efficiency accompanied by a reduction in cost of electricity by 15 – 28%, over conventional IGCC systems. Therefore, SCL process provides the best route to harness the energy from coal.

The overall project objective was to construct and operate a syngas chemical looping pilot scale test unit at the NCCC. The project scope of work was divided into 3 phases. In Phase I, cold flow model studies using a 1:1 scale acrylic test unit constructed at Particulate Solids Research, Inc. (PSRI) was successfully completed confirming robust solid flow control is achievable in the non-mechanical system design. In Phase II, the high pressure, high temperature, chemical looping reactor was successfully designed with all necessary equipment and safety instrumentation/controls specified to allow for fabrication, site construction, and assembly to commence in Phase III. In Phase III, the SCL pilot plant was successfully assembled and all necessary functional checks and pre-startup safety reviews completed. During unit commission over the course of 200 hours of testing, operational issues were observed with premix burner used for system startup. With the grants awarded by the National Energy Laboratory (NETL) and the Ohio Development Services Agency (ODSA) under awards DE-FE0023915 and D-14-18, the SCL pilot unit underwent three auxiliary equipment modifications to resolve all of the startup operational issues encountered. The unit was successfully demonstrated with 300+hr continuous operation. Key results obtained include high syngas conversion of 97.95% with 16.03% oxygen carrier conversion in the moving bed reducer and >99% purity H_2 produced from the moving bed oxidizer.

Contents

Executive Summary

The Syngas Chemical Looping (SCL) process developed by The Ohio State University (OSU) uses an iron-based oxygen carrier to convert syngas into high-purity hydrogen while simultaneously capturing sequestration-ready carbon dioxide. The unique gas-solid contact pattern of the counter-current moving bed design of the SCL reducer allows the fully oxidized iron oxide (Fe_2O_3) in the oxygen carrier particles to be reduced to a lower oxidation state of Fe/FeO without the thermodynamic constraints. The high iron oxide conversion achieved in the reducer minimizes the solid circulation rate required to maintain high syngas conversion in the process. A 250 kW$_{th}$ pilot demonstration unit based on this concept was designed and constructed at the National Carbon Capture Center (NCCC) in Wilsonville, Alabama.

The goal of this project was to operate the unit for extended duration for syngas conversion and hydrogen generation. In order to startup the unit and maintain steady-state operation, multiple auxiliary components were designed, commissioned and tested in the first 320-hour of cold/hot circulation campaigns. 4 hours of 350 lb/hr syngas injection was performed at ~1500˚F average system temperature. High carbon capture efficiency of >98% was achieved, while maintaining the pressure balance and gas sealing between each reactor.

In the final campaign of April 2017, the system was operated at higher temperature of 1700°F. The total operation duration was 305 hours, including 33 hours of syngas injection and 0.8 hour of steam injection. Pure hydrogen was successfully produced from the oxidizer reactor with no contamination of carbonaceous species including carbon monoxide CO and CO_2. The oxygen carrier particle make-up was negligible and was estimated to be less than 0.02 weight percent per hour (wt%-h^{-1}) from the baghouse fines collection.

As an advanced fossil fuel conversion process for high purity hydrogen production with in-situ carbon capture, the SCL Pilot Unit operations have demonstrated the superb performance of OSU's chemical looping system design, which features counter-current moving bed reducer/oxidizer and iron-based oxygen carrier particles with high durability.

Introduction

Coal is one of the major sources of energy today and more than 40% of electricity in the world is produced from coal. Even in the US, coal constitutes 50% for electricity generation. Coal combustion and coal gasification are the two main processes for utilization of coal as an energy source. Coal combustion is practiced in pulverized coal (PC) power plants which account for over 90% of the electricity generated from coal. It involves the burning of pulverized coal in boilers using air to generate heat which in turn is used for the generating steam to be used in steam turbines for producing electricity. The PC plants are however plagued with problems of low energy efficiency, poor control over pollutants and energy intensive CO_2 capture systems. Coal gasification, on the other hand, present an easier scheme for the capture and management of pollutants and CO_2. Coal gasification is a relatively new process scheme compared to coal combustion. It involves the partial oxidation of coal to syngas, as opposed to total oxidation in coal combustion, in a gasifier through the use of either steam, CO_2, oxygen or any combination of them. The syngas produced then offers a flexible option of either producing chemicals or liquid fuels or producing hydrogen and electricity. The syngas route to producing hydrogen and electricity is commonly known as the Integrated Gasification Combined Cycle (IGCC). In view of better carbon management, the syngas in an IGCC plant is first made to undergo a water gas shift reaction to convert CO into CO_2 which is later captured through chemical absorption or physical absorption techniques. This CO_2 capture strategy however decreases the energy efficiency of the IGCC process by 13-24% thereby increasing the cost of electricity by 25-45%. In order to make IGCC a cost and energetically competitive process there was a requirement for a more energy efficient process for capturing the CO_2. Chemical looping, more specifically syngas chemical looping, provides that energy efficient method for capturing CO_2.

At OSU, SCL process has been successfully demonstrated in the bench unit and sub-pilot scale unit, and techno-economic analysis revealed its improved performance compared to conventional technologies. This prompted the need to demonstrate the SCL process under a pilot scale with the simultaneous operation of all the three main reactors, namely the reducer, oxidizer, and combustor. Hence, the focus this project was to design, construct, and demonstrate Ohio State's Syngas Chemical Looping technology for carbon capture and hydrogen generation at a 250 kW$_{th}$ fuel input scale using synthesis gas from the KBR transport gasifier at the National Carbon Capture Center in Wilsonville, Alabama.

OSU was assisted by several important agencies like Babcock and Wilcox Power Generation Group (B&W), Particulate Solids Research Incorporated (PSRI), Shell/CRI, Air Products, and CONSOL Energy, who were the cosponsors for this project. B&W, in the first phase of the project was involved in developing the preliminary P&ID based on the functional document prepared by OSU and B&W. They also did a preliminary cost estimate for the unit construction and set up at the NCCC site. In phase II and III of the project, they assisted OSU in finalizing the P&IDs based on updates in the functional documents related to changes in operational and control procedures and also based on recommendation from HAZOP review done in collaboration with OSU, NCCC and UNWIN company. Activities related to the detailed mechanical design and finalizing fabrication of equipment was also facilitated by B&W. They in collaboration with NCCC came up with the construction, operation and commissioning schedule of the unit at the site location. Particulate Solids Research Incorporated (PSRI) assisted in designing and fabricating of the Cold Flow Model and finalizing the cold model test plan based on the hot model operating conditions. Shell/CRI, Air Products, CONSOL Energy and B&W were also part of the Industrial Review Committee and were

responsible for evaluation of the project process and providing important feedback and suggestions to resolve critical issues.

Technical discussion

The process is described in Figure 1 below. The SCL pilot unit consists of three reactors: a reducer, an oxidizer, and a combustor. The reducer reactor converts the syngas to CO_2/H_2O while reducing the oxygen carrier (Fe_2O_3) to a lower oxidation state (Fe/FeO). The reducer is capable of generating a sequestration-ready stream of CO_2 and capturing all of the carbon put into the system. The oxidizer partially re-oxidizes the oxygen carrier from Fe/FeO to Fe_3O_4 oxidation state with steam while generating H_2 in the gas product stream. Hydrogen generated in this stream is nearly 100% pure. The combustor fully re-oxidizes the oxygen carrier particles to Fe_2O_3 while producing heat and oxygen depleted air. Above the combustor, the riser pneumatically conveys the oxygen carrier to the top of the process through the primary particle separator (PPS). The PPS separates the oxygen-depleted air stream from the solid particles similar to a cyclone. Overall, OSU's syngas chemical looping process has the ability to completely combust syngas into pure CO_2 in the absence of nitrogen while producing a nearly pure stream of H_2. Through the reactor design, CO_2 is inherently separated from N_2 and no additional CO_2/N_2 separation steps are required.
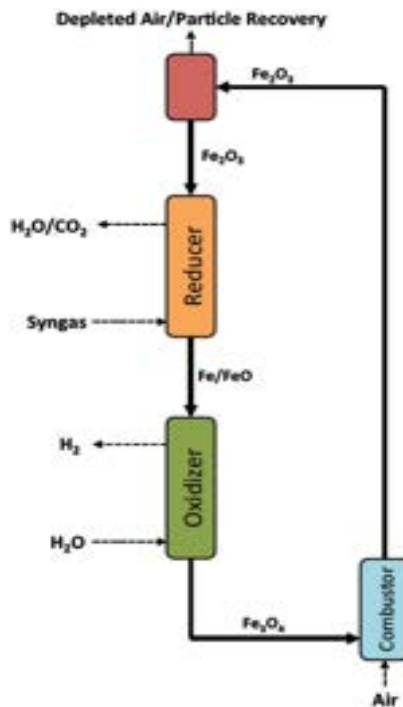
Figure 1. Syngas Chemical Looping process for hydrogen production and carbon capture.

The process described above has been carried out at the 25 kW_{th} sub-pilot scale unit located at OSU. In order to demonstrate the SCL process at a larger scale a 250 kW_{th} – 3 MW_{th} pilot scale unit has been constructed at the National Carbon Capture Center (NCCC) site which is operated by Southern Company. NCCC has a TRIG gasifier which has been used to process a wide range of lignite, sub-bituminous, and bituminous coals to produce syngas for use of multiple syngas or pre-combustion carbon capture projects research projects including the SCL pilot plant. A thermal oxidizer is available at NCCC to condition all unused syngas produced from the gasifier and the reducer, oxidizer and combustor gas outlet products from

the chemical looping plant prior to being vented to atmosphere. All the utilities required by the unit like steam, nitrogen, propane, compressed air and cooling water are provided by the site. Various aspects related to the construction and operation of the SCL unit has been described in sections 3 and 5.

The techno-economic analysis is presented in section 6. This analysis as shown in section 6.3 of this report assumes a coal processing basis of 132.9 tones per hour to provide syngas to the SCL system. We consider two distinct strategies for Sulfur handling using the SCL system. First consistent with the study in section 6.3, a warm gas cleanup unit with ZnO sorbent will produce ~10tons/hr of dilute sulfuric acid. Testing has also shown that the oxygen carrier used in the SCL system can handle H_2S and convert it to SO_2 with near complete efficiency. In that scenario, a flue gas desulfurization unit (FGD) with Calcium based sorbent will be used to capture sulfur in the form of CaSO4. In both the scenarios, sulfur will be captured and can achieve a low emission rate of <4 ppmvd. The NOx levels of pollution from the combustion process, are limited by Nitrogen dilution to less than 15ppmvd. The NOx levels are maintained at a low value by most of the ammonia from the gasifier being captured in condensate stream in the syngas cleanup. The mercury in syngas from the coal gasifier is captured in a carbon bed; the HCl is captured using Na_2CO_3. The ash produced is ~12.89 tons/hr and is proposed to dispose in a waste management unit that is capped to prevent exposure to atmosphere and has an active groundwater quality monitoring system. The iron oxide-based solids circulation rate is ~1550 tonnes per hour. An attrition rate of less than .02% has been experimentally demonstrated in the pilot scale system. Assuming this rate for the commercial scale system, if the attrited oxygen carrier is purged, 0.31 tonnes/hr is expected to be disposed of. Studies with attrited oxygen carriers from system demonstration have revealed that all the attrited material can be re-synthesized to appropriate particle size and reactivity. In this scenario, the purge stream flowrate for the Fe_2O_3 oxygen carrier is less than 0.001 tonnes/hr.

Studies with attrited oxygen carriers from system demonstration have revealed that all the attrited material can be re-synthesized to appropriate particle size and reactivity. The cost for resynthesizing the attrited oxygen carrier to an average size of 1.5 mm is less than synthesizing the oxygen carrier from fine powder starting material. This is because the average particle size of the attrited oxygen carrier material is ~600 microns, while that for powder is <100 microns. The cost for that operation is estimated to result in a 35% cost reduction in the required selling price of the oxygen carrier. A preliminary cost estimate of ~400$/tonne is assessed for the same. The cost of slag from the gasifier is determined using guidance from DOE/NETL baseline study as being $17.89/tonne and results in a cost of $230.6/hr based on the mass balanced based flowrates calculated above. The model in the base case conservatively assumed no credit for selling sulfur, gypsum or sulfuric acid. However, a cash flow of $30/short ton of sulfuric acid could be expected if that market is sought. For the option containing gypsum, a selling price of $7/ton may be assumed for crude gypsum or $20/ton for calcined gypsum. The spent Na_2CO_3 will have have a disposal cost that is similar to ash of $17.89/tonne. The waste disposal cost for carbon used in mercury control is based on guidance from DOE/NETL study and is costed to be $926/tonne. The basis for the techno-economic analysis are presented in section 6 and the background for values developed in the marketing plan is presented in section 7.

1. Project Management and Planning

Effective management of the time and people was key to developing the technology and meeting the milestones required for this project. Professor L.-S. Fan, the project principal investigator, was responsible for evaluating and approving IRC recommendations and supervising the overall research activities. Project management support from Clear Skies Consulting was able to assist Prof. Fan to coordinate the collaborations among the participants and to ensure that progress on each task was timely and updated to NETL and ODSA.

2. Burner Design, Fabrication, Installation and Testing

2.1. Complete detailed design and fabrication of pilot plant burner

The burner ignition experiments confirmed the burner was unable to operate due to the pressure fluctuations in the slugging bed combustor. Modifications were required to allow the burner to operate. Two approaches were applied:

1. Modify burner operation to withstand ±3 psi pressure fluctuation of the combustor reactor
2. Modify the burner chamber to dampen the pressure fluctuations the burner experiences

In the original burner, the fuel and air mix prior to entering the burner lance. The premix burner was limited in the pressure drop it can absorb. To perform option 1, Zeeco modified the premix burner to a raw gas burner to create a pressure drop at the burner lance tip greater than the pressure fluctuations in the combustor reactor. Figure 2 illustrates the raw gas burner design.
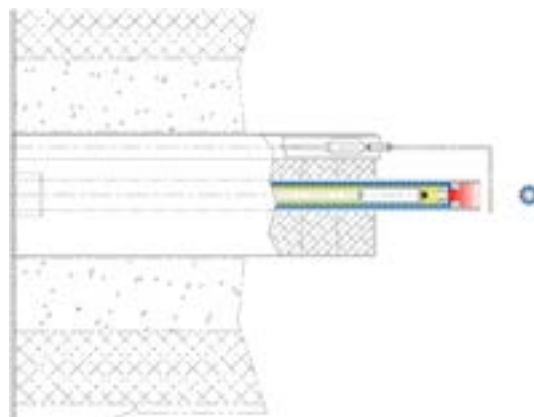
Figure 2. Raw gas burner design.

As illustrated, a concentric pipe is used where the fuel is introduced through the inner pipe (shaded yellow) and the air from the annular section (shaded blue). The burner tip is designed to create a pressure drop across the air and fuel supply to the vessel. The raw gas burner design minimizes the fabrication and assembly work. All modification work is contained within the 2" burner lance.

As shown in Figure 3, the raw gas burner design consists of three concentric tubes. The inner tube acts as the conduit for the propane gas and the wire for the high energy ignitor, and the propane exits out at the end of the tube through three holes, which are sized to allow for the correct stoichiometry of propane to the air. The middle concentric tube consists of the conduit for process air flow, and the tip consists of six holes. The exit holes are perpendicular to the central tube axis and are angled away from the center to allow the air to swirl and stabilize the flame. The holes for the air are large to accommodate a volumetric air to fuel ratio of at least 25 to 1 and to compensate for the lower supply pressure compared to the propane. The previous pre-mixed design only allowed for 10 inches of pressure drop across the tip. In comparison, the pressure drops across the propane and air orifices were designed around a nominal value of 50 and 30 psig. The tip of the burner also consists of a choke ring, which is a restriction that produces a small region for the air and propane to mix. Since the temperature of the flame is much higher than the stainless steel used for the flame guide tube, an outer layer of concentric piping provides a conduit for extra cooling air if required. The cooling air guide tube extends longer than the tip to provide a shroud of cooling over the entire tip. It was determined during testing that this air may not be necessary, as the process air through the main swirl could provide this cooling, but the air is kept in the design for safety.
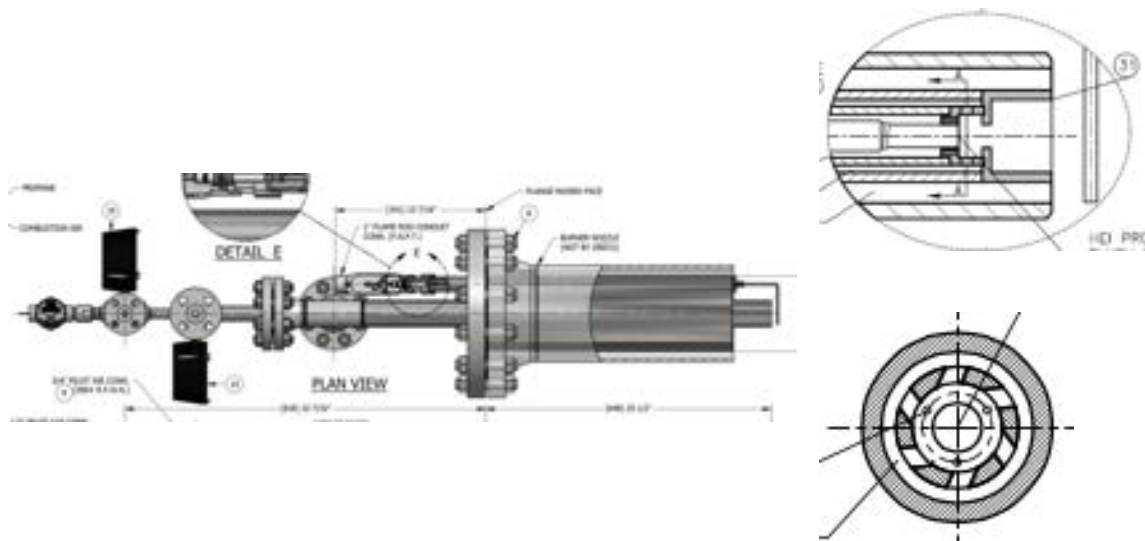

Figure 3. Redesigned burner for use in the pilot unit.

For option 2, the burner was placed at the entrance to the windbox. An extension piece is placed on the end of the windbox. The extension piece consists of expansion and constriction zones to dampen the pressure fluctuations experienced in the burner chamber.

2.2. Complete FAT with pilot plant burner

To more accurately test the pressurized condition of the pilot plant, a new testing vessel was constructed which provided for the full pressure of 150 psig found in the pilot plant vessel, as well as optimal observation of the flame and the process conditions. A sketch of the testing vessel is shown in **Figure 4**. The vessel consisted of a 15-foot water-cooled 8-inch pipe that leads to a series of manual valves, which can be adjusted to provide the desired pressure or pressure fluctuations. The vessel was designed to fit the 8-inch 300# flanged burner assembly. Four sight glasses were installed to be able to view the flame; three of them were spaced evenly along the predicted flame length, and one of them was placed at the end of the vessel to view the flame straight on. A number of ports were drilled for pressure measurement and for the addition of air to keep the sight glasses cool.
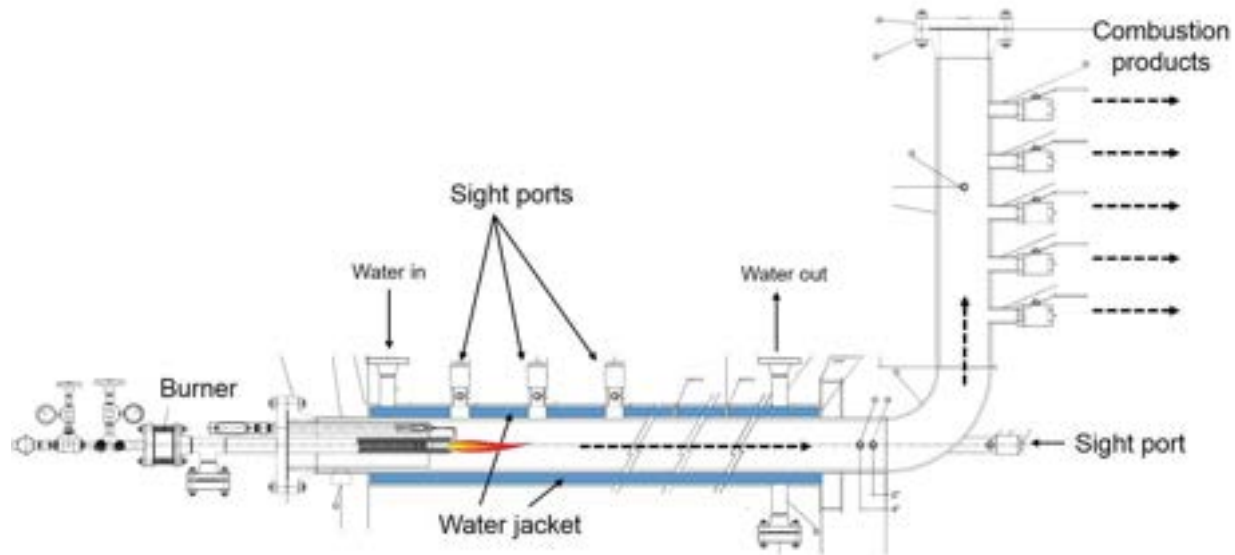
Figure 4. Pressure vessel designed for FAT test of burner.

The factory acceptance test took place at Zeeco's manufacture facility in Tulsa, Oklahoma. OSU and Babcocks & Wilcox observed Zeeco's demonstration of the burner operation at 90 psi (Figure 4). The guidelines for burner ignition and capacity modulation were determined:

1. During ignition, the flow rates of the fuel and combustion air should be set at 20% firing capacity (0.222 MM BTU/hr)

2. To increase the firing capacity of the burner, the flow rates of the fuel and combustion air should be ramped up in small increments such that the air to fuel molar ratio is maintained between 2 to 10% excess.

Figure 4. Factory acceptance test of raw gas burner in the simulated reactor chamber

Following these guidelines, the burner ignited and fired reliably at 90 psi vessel pressure. The robustness of the burner flame against pressure fluctuations was also tested and observed. The pressure fluctuations were simulated by opening and closing the manual ball valve at the vessel outlet, which generated pressure spikes around 1-3 psi. At low firing capacity (20%), the flame slightly diminished upon pressure build-up but stayed lit when the pressure went back to 90 psi. At medium and high firing capacity (50% and 75%), the flame was barely affected by the pressure fluctuations.

2.3. Pre-run preparation

A comprehensive hazardous operational review was conducted to ensure that the additional sections added to the vessel are adequately safe by design. The HAZOP consisted of reviewing the modified pilot unit with the new burner dampening chambers and the subsequent process instrumentation. A moderator from Unwin Company, a leading process safety consultancy, led the HAZOP discussion and documented the results. All of the parties involved that developed and specified design elements contributed to the meeting, including OSU, B&W, and Zeeco. The host site, the National Carbon Capture Center, was also involved to provide comments on site requirements and recommendations. A list of the major recommendations from the HAZOP are shown in Table 1, along with priority risk and responsible parties involved for solving the issue. Four of the issues pertaining to loss of burner process air that were revealed

in the HAZOP were considered to have adequate safeguards, namely temperature and pressure trips based on instrumentation. Furthermore, the comprehensive insulation inspection scheme developed previously was considered an extra layer of protection. Two of the issues involved a propane or process gas loss-of-containment scenario, mainly upstream of the burner management system and skid. If loss-of-containment were to occur downstream of the burner skid—between the outlet of the skid and the inlet of the burner, the skid instrumentation would be able to register the abnormal readings and trip the block valves of the propane. However, loss-of-containment upstream of the skid would not necessarily be registered by the burner management system. The main safeguard for loss of containment of propane included NFPA hazardous environment classification for electrical equipment, particularly Class I Division 2 requirements for all electrical equipment within a 30-foot radius within the structure. Further safeguards will be implemented. The remaining recommendations were based on process upsets that could cause damage to equipment but no hazards to personnel.

Table 1. List of new burner HAZOP recommendations with and without burner chamber.

Node	Priority Risk*	Recommendation	Responsible Party
Burner Chamber	C	Update control specifications document: (a) include burner interlock for insulation interface TE-221/222 w burner trip via main PLC.	OSU with B&W approval
""	C	Consider hardwired interlocks for insulation interface temperature (TE-221/222) to burner trip.	OSU with B&W approval
""	C	Confirm whether or not FCV-114 has minimum flow stop. Determine whether minimum flow prevents overheating downstream.	OSU/Zeeco
""	C	Confirm the air-to-fuel ratio logic control with Zeeco.	OSU with B&W/Zeeco approval
""	B	Confirm FCV-114 fail position with Zeeco. Verify fail safe condition for SDV-113.	OSU/Zeeco
""		Confirm with Zeeco the minimum air flow through burner to provide necessary cooling.	OSU/Zeeco
""		Confirm with Zeeco that the gas velocities in the fuel and air passages within the burner piping exceed the flame velocity for all ratios of fuel and air.	OSU/Zeeco

Combustor/ frustum		Determine setpoints of PT-140 HH and LL, and PT-118 HH and LL.	OSU/Zeeco
""		Confirm with Vesuvius the maximum differential pressure allowable for the orifice disks.	B&W
""		Consider adding a minimum flow stop on FCV-200 (N2 to Combustor) to prevent instantaneous depressurization during system trip. Update System Trip function to include driving FCV-200 to minimum flow stop.	OSU with B&W approval
Burner Chamber		Add system trip I-14 on PIT-221 HH (> 325 psig). Alarm on PDIT-222/223 at setpoint TBD.	OSU with B&W approval
Burner only	**B**	Reduce risk of flange assembly errors. Option for consideration: (A) perform leak check prior to startup; (B) include use of mobile hydrocarbon detection in startup SOP.	B&W

2.4.   Post-run pilot plant commissioning

The burner was shipped to the NCCC site after the successful factory acceptance test. Before assembling the burner to the alternate burner chamber, the functions of the igniter and the flame rod were tested with the energized burner control panel. The burner was then installed and leak-tested by OSU at all the flanged location with a combustible gas sniffer. The burner ignition tests were then performed with the system filled with particles. The test parameters for successful ignitions are summarized in Table 2. The raw gas burner was very robust in conjunction with the alternate burner chamber as the flame stayed lit stably after ignition (Figure 5 left). The side glass design also served as a good indicator for troubleshooting the burner. For example, when there is liquid propane residue in the line, the ignition is most likely inhibited. Visually the sparks of the ignition are more violent, and burning liquid drops can be observed (Figure 5 right).

Figure 5. Visual observation of the burner ignition operation.

Table 2. Burner test conditions

	Pressure (psig)	Combustor Air (lb/hr)	Solid Bed Mode	Burner Propane (SCFH)	Burner Air (SCFH)
Test 1	30	1000-1300	Fluidization	95	2200
Test 2	30	1300	Circulation	95	2200
Test 3	60	1400-1700	Circulation	90	2200
Test 4	60	1800	Circulation	90	2250
Test 5	60	1800	Circulation	85	2250
Test 6	90	1900	Circulation	102	2900
Test 7	90	1900	Circulation	102	2900
Test 8	90	1900	Circulation	102	2670

3. Alternate Burner Chamber Design, Fabrication, Installation and Testing

3.1.   Alternate Burner chamber detailed design

The intent of the chamber orifices was to build pressure upstream of the strong pressure fluctuations in the combustor reactor of the system. To understand the burner flame stability problem and to provide sizing for the chambers, OSU developed a chamber flow orifice model that estimated the dampening effect as well as the effects on flame stoichiometry. The model performed a differential mass balance of the gases entering and exiting each chamber, where the mass flow calculations used standard compressible-flow orifice equations based on the upstream and downstream pressures. The model mimicked the same control

of the burner skid, with the propane pressure controlled to a certain pressure difference above the vessel, and the air pressure at a certain differential pressure above the propane pressure. This setup is shown in Figure 6. Furthermore, the downstream vessel pressure is modeled assuming a sine wave with the same amplitude and frequency as the fluctuations found in the slugging combustor.

OSU verified the orifice calculations in the model by comparing the flow of air and propane exiting the burner orifices to that specified by Zeeco. For example, the flow calculated through the propane orifice at 100% capacity was 1.087 MMBTU/h, while the design flow was 1.109 MMBTU/h, which was an error of 2%. The air flow was also validated at different ranges of stoichiometry based on the set point pressure of the air compared to the propane. OSU also validated the model using small acrylic chambers and orifices in a fluidized bed cold model with reasonable correlation.
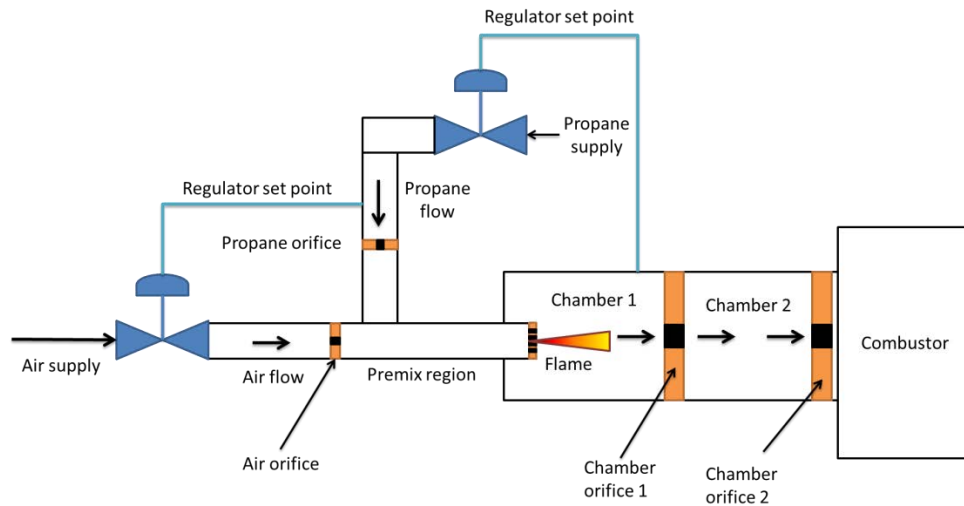

Figure 6. Chamber used for mass balance model.

Figure 7 shows the pressure plot of one of the simulations using a single chamber dampener. The upper left-hand graph shows the downstream pressure, the chamber pressure, and the propane and air pressures as a function of time. The upper right-hand corner graph shows the flow rates of the air, propane, and mass flow out of the chamber as a function of time. The lower left-hand graph shows the temperature of the chamber, and the lower right-hand graph shows the molar ratio of air to propane. As the pressure graph shows, once the temperature plateaus at 1600 K, the pressure of the vessel fluctuates between 131 to 134 psig, while the chamber pressure only fluctuates between 144.97 and 145.23. This is a 91% reduction in pressure fluctuation. Furthermore, the molar ratio of the air to propane is shown to be steady once the temperature lines out.
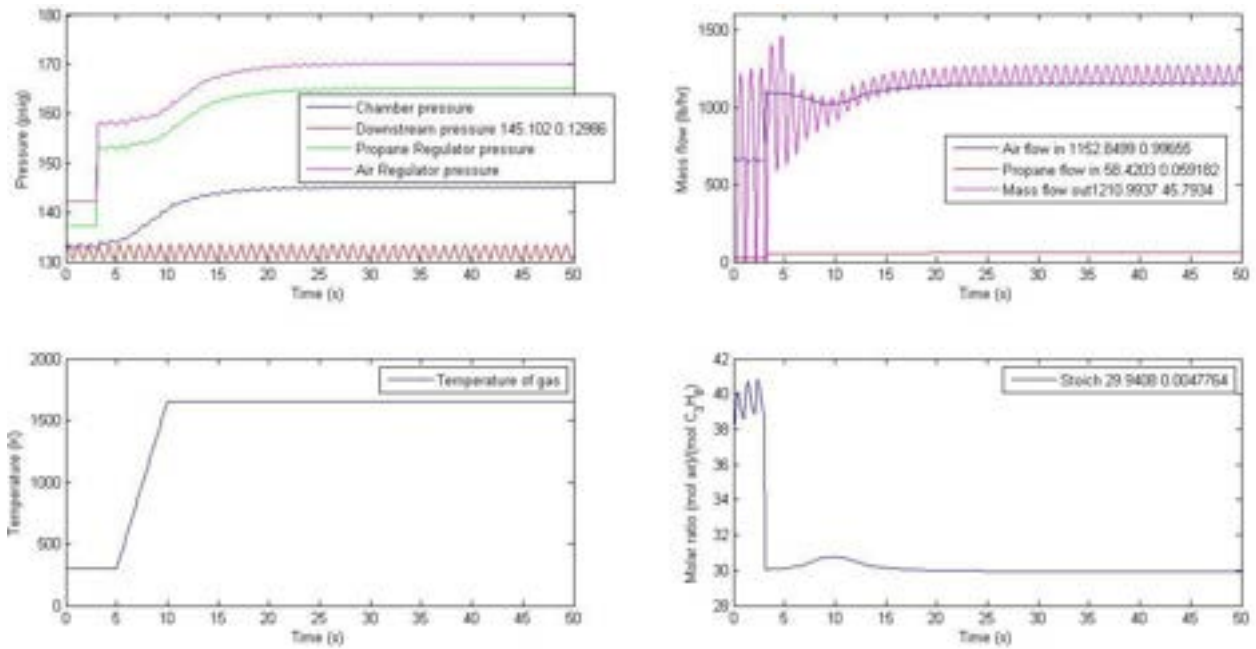
Figure 7. Plots showing the dynamics of the vessel fluctuations on a single dampening chamber for the burner.

Figure 8 shows the effects of the volume of a single chamber and a second chamber in series with the flow of the first chamber. As the chamber volumes increase, the pressure fluctuations decrease from 3 psi at 0 L to less than 0.3 psi at 500 L. The number of orifices in the chamber further decreases the fluctuations but increases the upstream pressure required for the air and the propane. Based on the analysis, OSU determined the size of the chamber, the number of orifices, and the orifice size based on how much fluctuation attenuation was required for the burner as well as the space limitations at the site.
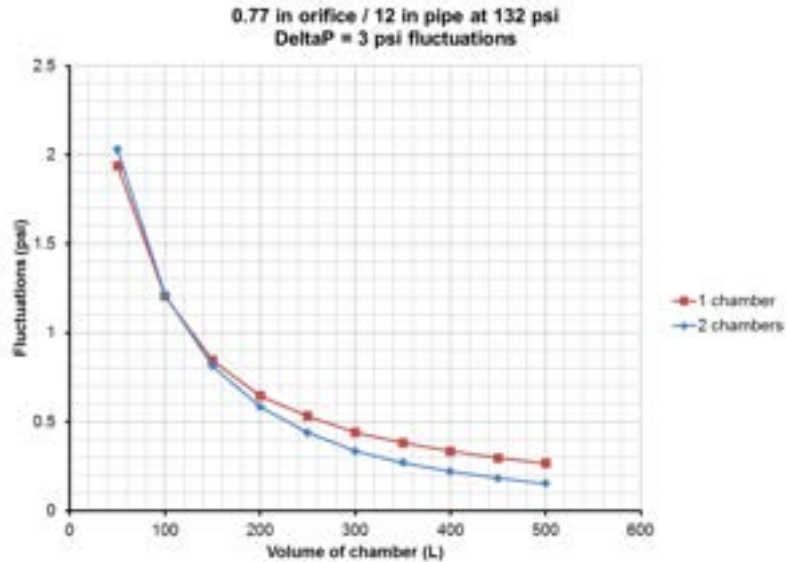
Figure 8. Effect of chamber volume on the upstream fluctuations.

3.2. Alternate burner chamber fabrication and assembly

B&W solicited two vendors for quotes for the shell fabrication: McAbee Construction in Tuscaloosa, Alabama and Gaspar, Inc. of Canton, Ohio. After quotes were solicited, Gaspar, Inc. was selected for the alternate burner chamber fabrication, and the PO contract was completed at the end of Q4 of 2014. Gaspar initiated the material procurement of the shell piping and flanges after the PO contract was signed. For the insulation vendor, Vesuvius was also selected at the end of Q4 of 2014.

Gaspar procured the materials for and constructed the alternate burner chamber vessel based on drawings provided by Babcock and Wilcox provided in the previous reporting period. The windbox shell material procurement was initiated in Q4 of 2014, and fabrication and hydrotesting was successfully completed at the end of January. Representatives from OSU and B&W were present to witness the pressure vessel hydrotest and stamping per requirements of ASME Boiler and Pressure Vessel Code, Section VIII, Division 1. Figure 9 illustrates the assembled windbox during the hydrotest. At the completion of the pressure vessel certification, the vessel shell was packaged and delivered to Vesuvius.

Figure 9. Picture of hydrotesting of burner chamber shell at Gaspar, Inc.

After Vesuvius finished the insulating the burner, the chambers were shipped to the site with special instructions for assembly. The burner chamber assembly shipped and arrived on site in the middle of March. OSU hired McAbee Construction to remove the old windbox installed on the pilot plant vessel and install the new burner chamber to the pilot plant along with the supports specified and procured by B&W.

Prior to the installation of the alternate windbox, high temperature dryout of the overall reactor vessel was performed. Hotwork was contracted by B&W to perform the reactor dryout. Propane burners were placed below the combustor chamber and the moving bed reactors where the combustion gases were discharged from each of the 3 gas outlets. Vesuvius provided the ramp rate and holding point temperatures. At the completion of the high temperature dryout, the alternate burner chamber was immediately installed to prevent moisture ingress into the reactor vessels.

After unloading the chambers off the truck using a special fork-lift, the windbox distributor was lined with high-temperature mortar and carefully placed into the tee. The horizontal pipe and tee were then lifted into place in the vessel with the forklift and chain falls. Ceramic and stainless steel gaskets were then installed between the flanges. The flanges were then tightened according to Babcock and Wilcox's bolt torqueing procedure. Once the vessel supports were installed, which consisted of a spring can dampener and a lateral support, the chain falls were removed.

3.3.   Prerun preparation and pilot plant operation

After installation of the burner chamber windbox and orifices, the system underwent shakedown to test the various components. The setup consisted of a burner at the end of the chamber, tangential attemperating air injection, which provides a stabilizing swirl for the burner, two ceramic orifices to build backpressure at the burner and attenuate the pressure fluctuations at the windbox, and a ceramic distributor plate that can withstand the heat from the burner. The chambers also consisted of a number of temperature, pressure, and flame measurements for safety and controllability.

The main goals of this operation were to demonstrate that 1) the windbox/chamber assembly provides the designed function for stable solid fluidization and entrainment, and 2) the pressure fluctuation damping effect across the chamber orifices. The operation of the alternate burner chamber was successful. Solid circulations were performed under 30 and 60 psi, and steady states with desired pressure balances of each reactor were maintained for extended periods of time. The absolute pressures of the burner compartment and of the combustor were recorded with different sets of pressure transducers to ensure the experiment consistency.

Before the addition of solids to the vessel, the installed vessel was tested by flowing medium pressure nitrogen through the new windbox and orifices. These flow tests were needed to confirm that the predicted pressure drops are as expected based on orifice flow calculations. If the pressure drops were too high, the orifices would need to be sized larger; however, this was shown not to be the case. Furthermore, the pressure drop and flow correlation needed to be confirmed for correct comparison of the orifice attenuation model. The calculations for the model are shown below.

The pressure drop across an orifice whose flow can be considered incompressible is

$$\Delta P = \frac{K_0 R T_1}{2 P_1 M} \left(\frac{\dot{m}}{A}\right)^2 \qquad (1)$$

where K_0 is the loss coefficient calculated based on the thick orifice correlation suggested by Rennels and Hudson (2012), P_1 and T_1 are the gas pressure and temperature upstream, respectively, $\dot{m}$ is the mass flow rate, and A is the orifice area. The loss coefficient is defined as

$$K_0 = 0.0696(1 - \beta^5)\lambda^2 + (\lambda - 1)^2 + (1 - \beta^2)^2 + f_0 \left(\frac{t}{d_0} - 1.4\right) \qquad (2)$$

where β is the ratio of the orifice diameter (d_0) to the pipe diameter, f_0 is the friction factor (roughly assumed as an average value for simplification in the calculations), and t is the orifice thickness. The jet contraction coefficient (λ) is based on the ratio of the inner orifice diameter to the pipe diameter and defined as:

$$\lambda = 1 + 0.622(1 - 0.215\beta^2 - 0.785\beta^5) \qquad (3)$$

Since the flow through the orifices is well below the speed of sound (the Mach number was calculated to be less than 0.16, which is less than the incompressible 0.3 threshold), the flow can be considered incompressible, and the above equation can be used without an expansion factor. Thus, it can be safely assumed that the properties in the pressure drop calculations only need to be based on the upstream

pressure only. Table 3 shows the properties of the orifices and the constants used for the orifice flow calculations, which are independent of flowrate.

Table 3. Properties of the two installed ceramic orifices.

Orifice diameter (d_0)	1.1 inch
Chamber inner diameter	12 inch
Orifice/Chamber diameters (β)	0.09167
Ceramic orifice thickness (t)	4 inch
Friction factor (Averaged) (f_0)	~0.005
Jet contraction coefficient (λ)*	1.62087
Loss coefficient (K_0)**	1.56278

*Defined as: $\lambda = 1 + 0.622(1 - 0.215\beta^2 - 0.785\beta^5)$, from Rennels and Hudson, 2012.
**Defined as: $K_0 = 0.0696(1 - \beta^5)\lambda^2 + (\lambda - 1)^2 + (1 - \beta^2)^2 + f_0\left(\frac{t}{d_0} - 1.4\right)$, from Rennels and Hudson, 2012.

Measurements of the pressure drop across the orifice as a function of nitrogen flow rate in the absence of fluidized solids were taken. Figure 10 shows a plot of the flow through the orifice versus the pressure drop for vessel pressures around 30 psig and 60 psig. Nitrogen was used because the facility could provide a finer control of nitrogen flow rate compared to air, which is supplied by an air compressor which cycles at low flow rates. The curves which show the predicted pressure drop as a function of flowrate coincide relatively closely with the measured pressures, showing that the engineering calculations were correct. This also implies that the pressure drop of the orifices does not prevent maximum air flow required for the process. Thus, the orifices are sized correctly to allow for maximum flow of air while allowing maximum attenuation of the frustum fluctuations.

The orifice hole diameter was designed to be one inch, but the calculations showed that the orifice diameter fit the data better using 1.1 inches as the hole size based on a least-squares fit. This is due to the fact that the predicted pressure drop is most sensitive to the orifice diameter, whereby the pressure drop is proportional to the inverse orifice diameter to the fourth power. This difference can most likely be due to the manufacturing technique, which required a 1-inch tube to cast the ceramic orifice. The value of 1.1 inches was thus subsequently used for the orifice attenuation model for further study.
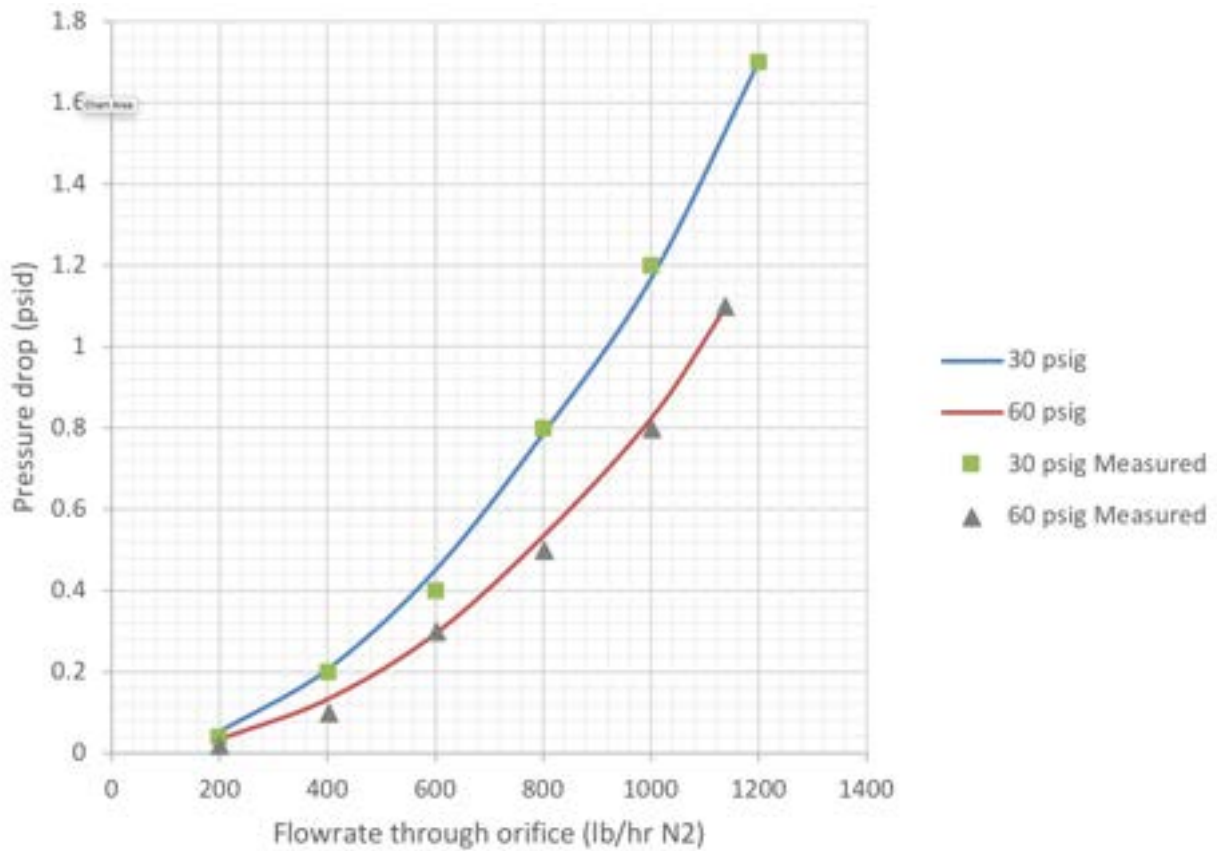
Figure 10. Flowrate of nitrogen through the first orifice versus calculated or measured pressure drop.

The effect of the orifices in the burner chambers can be seen in Figure 17. The frustum pressure fluctuations are shown in Figure 11(a) for the condition of cold solids circulation. The frustum air flow rate is set at 1.73 times the minimum fluidization velocity in the combustor and 1.11 times the terminal velocity in the riser. From the figure, it can be seen that there exist occasional peaks that reach as high as 2 psid above the steady pressure conditions. This can be interpreted as a slug of solids being entrained into the riser. Overall, the time-averaged fluctuations are shown to be 1.30 psid, which include the small fluctuations from fluidization of the particle and the large fluctuations from slugs entering the riser.

Plotted on the same time scale and differential ordinate in Figure 11(b) are the pressure fluctuations in the burner chamber region. Qualitatively, it is shown that the fluctuation patterns are similar in shape and follow the fluctuations in the combustor and riser, but the magnitude of the pressure fluctuations is drastically reduced as a result of the installed attenuating orifices. Some of the jumps could also be interpreted as a result of the loading and unloading cycles of one of the stages in the air compressor.

Combustor pressure
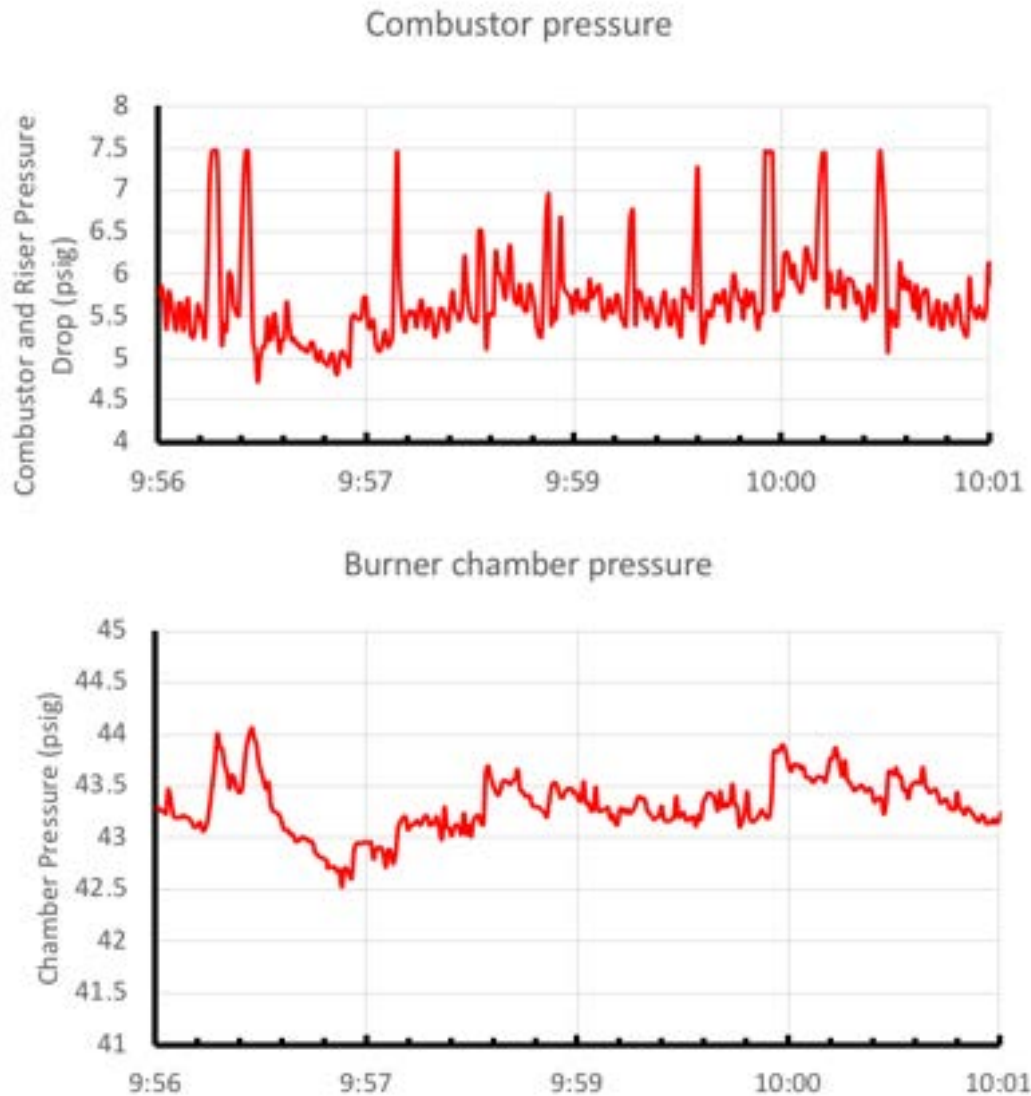

Burner chamber pressure

Figure 11. (a) Differential pressure measurements in the combustor and riser, (b) Pressure measurements in the burner chamber region upstream of the attenuating orifices.

The time-averaged pressure fluctuations measured in the upstream burner chamber and the combustor are compared to the pressure fluctuations obtained from the orifice attenuation simulation. Table 4. Comparison of pressure fluctuations found in the system versus the expected reduction. shows a comparison of the experimental results to the simulation results. The input to the attenuation simulation was a sine wave of amplitude of 1.30 psid with a frequency of 1 Hz and an offset value equal to the gauge pressure in the frustum at the distributor (which was 35 psig). As shown in the table, the predicted difference between maximum and minimum pressure was around 0.27 psid resulting in an attenuation of 67.9%, while the actual difference was 0.42 psid with an attenuation of 59.1%. This results in a relative error of 15%, which is a fairly good prediction considering the uncertainties in the design calculations. This information has been repeated with other data cross sections. The predicted upstream pressure in Table 2

shows a predicted minimum chamber pressure of 40.3 psig, while the actual results show a minimum chamber pressure around 42.5 psig. This is fairly close to the predicted, around 5% relative error. The simulation does not take into account the pressure drop across the distributor plate and the coarse topping material, which is difficult to predict due to the complicated geometry.

Table 4. Comparison of pressure fluctuations found in the system versus the expected reduction.

Pressure	Min (Simulation)	Max (Simulation)	Predicted Difference (Simulation)	Actual Difference (System)
Frustum Pressure	34.3689	35.6309	1.3054 psid	1.3054 psid
Chamber Pressure	40.3395	40.6088	0.26929 psid	0.41845 psid
Percent Reduction	--	--	67.9%	59.1%

Reasons for difference between the model and the real system are as follows. First, the fluctuations in the simulation are assumed to be from a smooth, continuous sine wave, while the fluctuations in the real system resemble pulses and step functions. Work in the future will attempt to input actual frustum fluctuation data to compare more rigorously. A second source of error is introduced due to the fact that air flow entering the chamber is not fully developed. In general, the source of air should be introduced between 20 to 40 pipe diameters upstream of the orifice, but because of lack of footprint, this could not be achieved. This is also not a necessary requirement since the goal is to attenuate the downstream fluctuations, but this requirement would help make studying the system more scientific. Similarly, it is possible that the spacing between the orifice plates does not accommodate for the flow to become fully developed, which would result in a different jet contraction coefficient correlation. Third, the model also does not take into account the pressure drop across the distributor plate and topping material. In principle, the greater the upstream pressure, the greater the attenuation effect due to the fact that the gas is denser, allowing for more gas to be held up in the upstream chambers. Other minor factors include error in measurement of the pressure transmitters and the flow rate in from the flow control valve.

At the beginning, the 7 CFM tests similar to that for the dummy particles were performed. The experimental data of gas velocities, pressure distributions in the system as well as the performances of the zone seals were recorded and analyzed. The pressure drops in the reducer, oxidizer, L-Valve, combustor and riser were compared with the expected values estimated by corresponding theoretical calculations.

The CFM tests carried out successfully covered all the operational conditions for the tests in the hot unit. Therefore, these results indicate the robustness of the proposed design and control strategy. The experimental results concluded that a zone seal gas flow rate that was less than 2% of the gas flow rate in the reducer was adequate for safe and reliable operation.

The CFM performed well under all the testing conditions including the extreme operational conditions, such as highest and lowest gas flow rates, largest and smallest pressure imbalances between the left-hand side and right hand side of the system. Due to slightly different hydrodynamic properties of iron oxide particles, a higher pressure drop in the frustum was observed when iron oxide particles were used in the CFM instead of glass beads. This leads to higher than expected residence time of iron oxide particles in the frustum. Thus, the solids level and pressure drop in the frustum were decreased to the original values. The observation from the experiment showed that this modification also decreased the pressure fluctuation in the frustum.

The alternate burner chamber was tested at the full operating pressure range under solid circulation conditions. As illustrated in Figure 12, the alternate burner chamber was able to reduce the overall pressure fluctuation by over 70% consistent with the simulation results. During approximately 72 hours of the operation, the raw gas burner operated reliably under oxygen carrier circulation and pressurized conditions. Therefore, the raw gas burner and alternate burner chamber are considered robust to the pressure fluctuations of the fluidized bed combustor. The pilot unit was heated to 600°F prior to shutdown. The windbox gas temperature at the entrance of the combustor was 1,600°F (871°C). Success Criteria 1 was met as the FAT was successfully completed. Success Criteria 2 is considered incomplete as the reactor temperature of 700°C, or 1,292°F, was not met due to local temperature excursions alternate burner chamber shell during operation.
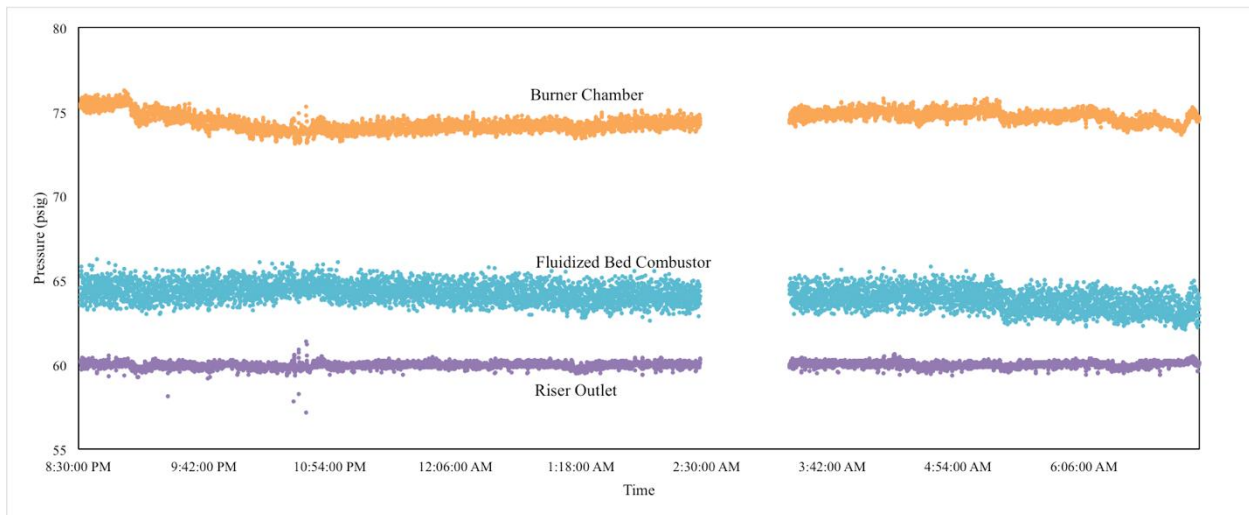

Figure 12. Pressure profile of the alternate burner chamber and combustor during hot solid circulation.
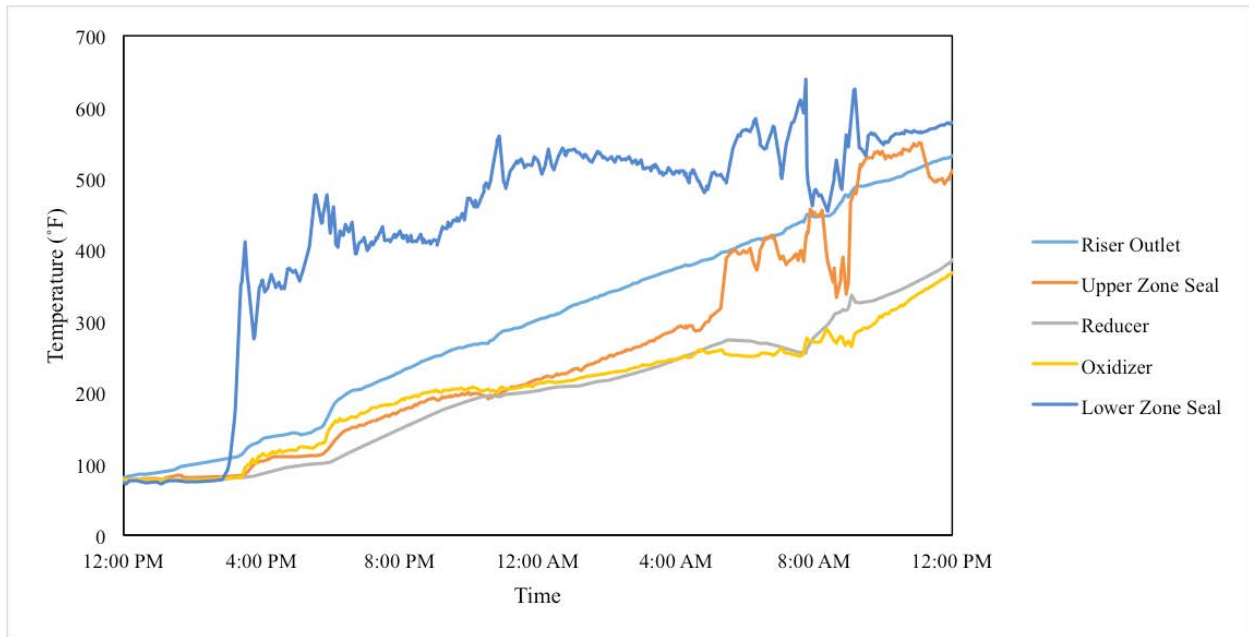
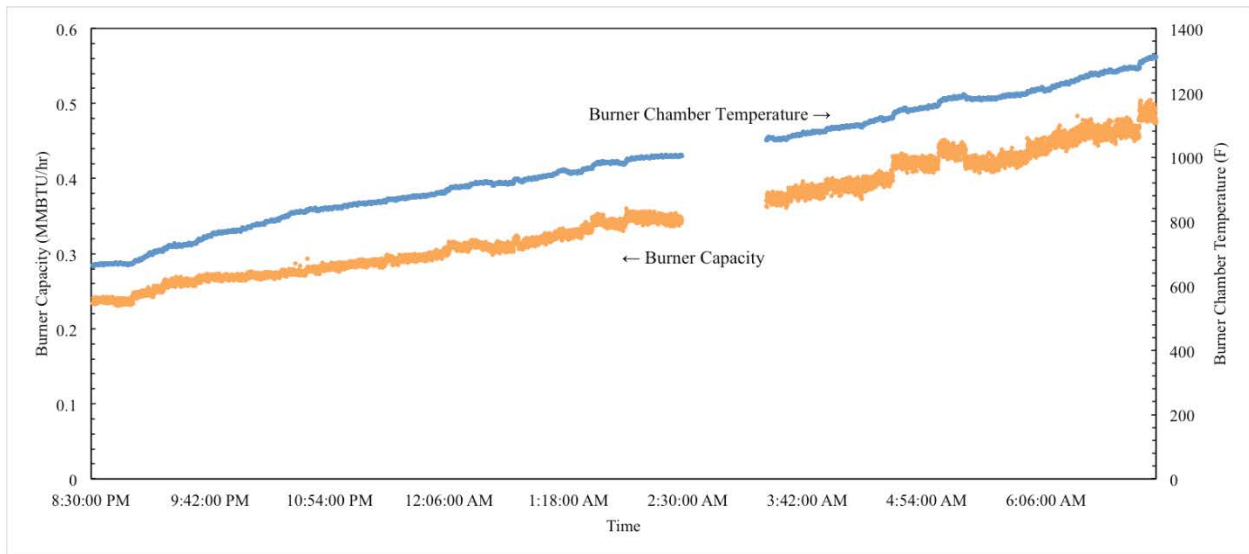Figure 13. Temperature profile of the hot circulation operation

Figure 14.Burner firing capacity and burner chamber temperature v.s. time.

3.4.   Postrun pilot plant commissioning

Referring to the burner test plan, at the completion of the empty combustor chamber and stationary fluidized bed burner startup testing, further test activities were performed to heat the oxygen carriers to

operating temperature under solid circulation conditions in preparation for the gasifier test run as indicated in the third tasks of the test plan. Local high temperatures areas were observed on the metal shell of alternate burner chamber at the pressure tap ports and near the plate discs installed, which were substantially higher than expected at the measured operating gas temperature in the chamber. Figure 15 is a photo from a thermal imaging camera taken during operation to indicate conceptually the local high temperature points. Figure 6 provides a conceptual temperature profile, while Type K thermocouples were used to measure the peak skin temperatures. The maximum skin temperature observed on the carbon steel shell was 450°F when the internal gas temperature near the combustor inlet was 1,600°F, which was approximately 200°F higher than the expected skin temperature at the given gas operating temperature. Further inspection and analysis using computational fluid dynamics indicated the most likely cause was due to vendor installation issues resulting in a small separation between two sections of the hard face material. The model results matched well with the temperature profile observed in the field as shown in Figure 16.
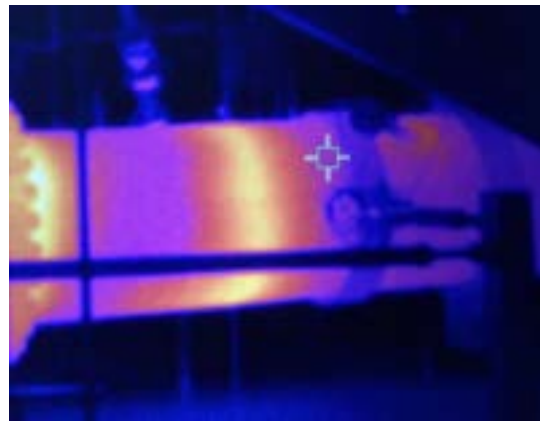

Figure 15. Thermal image of alternate burner chamber during operation.
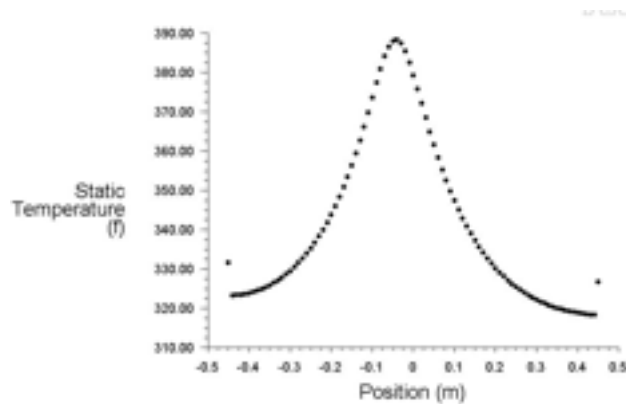

Figure 16. CFD simulation results for the temperature profile of the metal shell along the axial length of the burner chamber. Note, a 1mm separation of the hard surface is located at 0M position in this figure.

The local temperature excursions in the alternate burner chamber prevented the completion of the success criteria 2 in the SOPO as the reactor system could not reach operating temperature under solid circulation conditions as part of the third task in burner test plan. The simulation results indicate the design temperature of the alternate burner chamber limited the operating temperature of the gas from the burner chamber. Further, the heat loss from the shell resulted in operating the burner potentially above its design capacity. Therefore, in order to allow the completion of the startup activities and to fully understand the operation of all components upstream and downstream of the burner chamber, direct introduction of propane downstream of the alternate burner chamber was proposed.

4. Long Term Test Campaign One

4.1.   Downstream propane lances installation

The two lances were designed to inject propane into the windbox chamber and the combustor frustum. The designed gas mixture temperatures for the windbox and combustor WERE 1922˚F and 2100˚F, respectively. Heat and material balance was updated to account for burner heat input and the expected heat loss in the burner chamber to determine the required propane for the propane injection ports. The required propane flow was used to determine the necessary orifice sizes in the propane lances to produce 5-10 psi of pressure difference across the propane lances and the reactor vessel to prevent reverse flow. Nitrogen is used in the burner lance to maintain the pressure difference across propane lance and vessel at varying operating capacities of propane used in the lance to provide flexibility in operation. The calculation also accounted for the heat transfer on the lances, making sure that the flow through the lances are sufficient to cool down the lance bodies.

The P&ID design of the propane injection was developed to incorporate all necessary safeguards such as check valves, shutoff control valves and temperature sensors. A PHA review of the updated P&ID was performed to ensure sufficient safeguards are in place to prevent the occurrence and/or mitigate the consequences of process deviations. Each propane lance consisted of two gas lines, propane and nitrogen. Two check valves were placed downstream of the gas mixing point to prevent flame from propagating further back. The pressure at this point was measured by pressure transmitters and compared against the vessel side pressures for the designed 5-10 psi differential. Both gas flow rates were controlled by needle valves, and the values were read from flow meters in the field.

A 1/4" type B thermocouple, which was rated up to 1800˚C, was used to measure the high temperature in the windbox chamber. On the other hand, a 1/4" type K thermocouple was used to measure the combustor temperature because a lower temperature was expected due to the mixing of hot gas and cold particles coming from the L-valve.

Two shut-off control valves were installed on each of the propane lines. Safety permissives and trips were programed to ensure the valves close automatically under potentially hazardous conditions to cut off propane injection. Both propane lines were heat-traced and insulated to minimize propane condensation. One 1/8" type K thermocouple was also installed on each propane line downstream of the shut-off valves

to monitor the propane temperature and prevent liquid propane condensation. The completed piping and control modification are shown in Figure 17.

Figure 17. Pictures of the completed lance modification.

To ensure the integrity of the lances in the combustion environment, Incoloy 800H was selected as the material to fabricate the lances. Incoloy 800H has the following characteristic:

1. High temperature strength

2. High creep rupture strength

3. Resistant to oxidation and carburization in high temperature environments

4. Good corrosion resistance in many acidic environments

5. Good resistance to many sulfur-containing atmospheres

Therefore, Incoloy 800H is normally used in temperatures above 1100°F where resistance to creep and rupture is required. The chemical balance allows the nickel steel alloy to exhibit excellent resistance to carburization and oxidation atmospheres.

The design of the lances are shown in Figure 18.The windbox lance was a 3/8" tubing inserted from the side of the windbox, perpendicular to the direction of the fluidizing/entraining air flow. The opening of the tip end was capped with welding material. At the tip the tubing, two 1/8" orifices point towards the same direction as the air flow. The two orifices located at the center line of the windbox provide a good propane distribution for combustion. The combustor lance is a 1/4" SCH 40 pipe inserted into the combustor through the guide tube of the removed pre-mix burner. Therefore, the lance points directly to the fluidized bed. The tip end is also capped with a threaded cap piece, which has a single 11/64" orifice in the center.
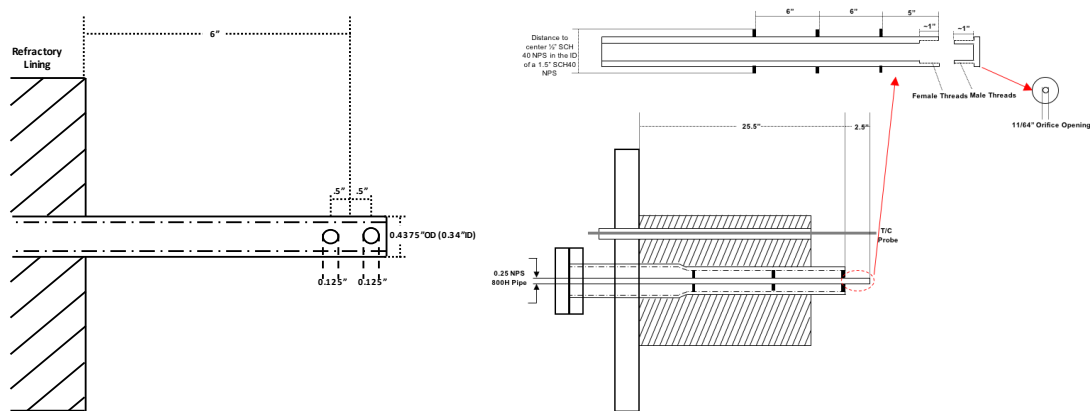
Figure 18. Windbox lance and combustor lance design

OSU performed a thorough testing on the leak test and functional test on all the components in the new modification. Nitrogen was used to pressurize the gas lines, and the gas lines were able to hold 80 psi for more than 3 hours with no leakage. With a Fluke pressure module, the instrument readings were tested and confirmed from the HMI. The safety features were also tested by simulated deviations using the Fluke signal device and/or RSLogix force masks. The modification was considered ready for operation in 2016 Q1.

4.2. Startup operation and secondary particle separator modification

A total of 3 startup runs were completed over a 96-hour operating period. The startup procedures were as follows:

Operation 1: Circulate solids at >300 lb/h and heat up system with electric gas heaters only.

Operation 2: Circulate solids at >300 lb/h and heat up system with electric gas heaters only while increasing back-pulse frequency to every 15 seconds on secondary particle separator.

Operation 3: Circulate solids at >300 lb/h and heat up system with electric gas heaters, propane burner and propane lances.

Continuous pressure buildup across the filter elements in the secondary particle separator was observed during Operation 1, as illustrated in Figure 19, which led to system shutdown because of over-pressurization. The suspected cause of the pressure buildup was either ineffectiveness of the back-pulsing system or moisture collecting on the solids. Therefore, 2 startup experiments were designed to test the performance of the secondary particle separator with and without moisture and with a modified back-pulse as described on Operation 2 and Operation 3.
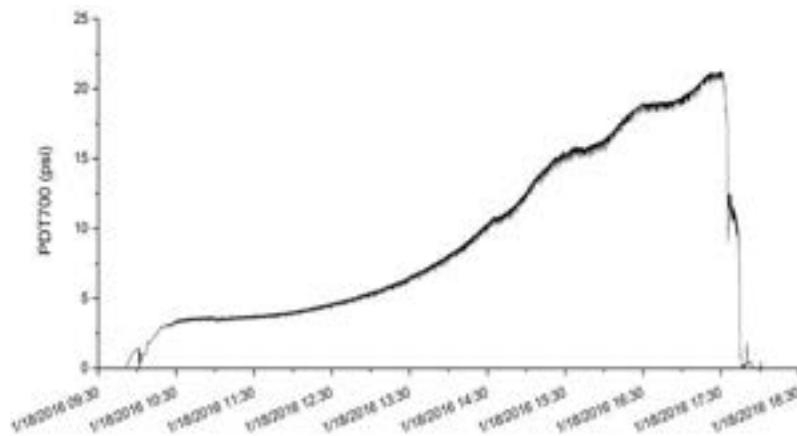
Figure 19. Differential pressure across secondary particle separator filter elements during Operation 1

As illustrated in Figure 20, the secondary particle separator consists of 7 sintered metal filters housed in a 24" ID vessel. A pressure differential transmitter is installed between the gas inlet (high leg) and the gas outlet (low leg), which is used to indicate the pressure drop across the 7 filter elements. An increase in the pressure across the secondary separator is an indication of fines accumulation on the filter elements.
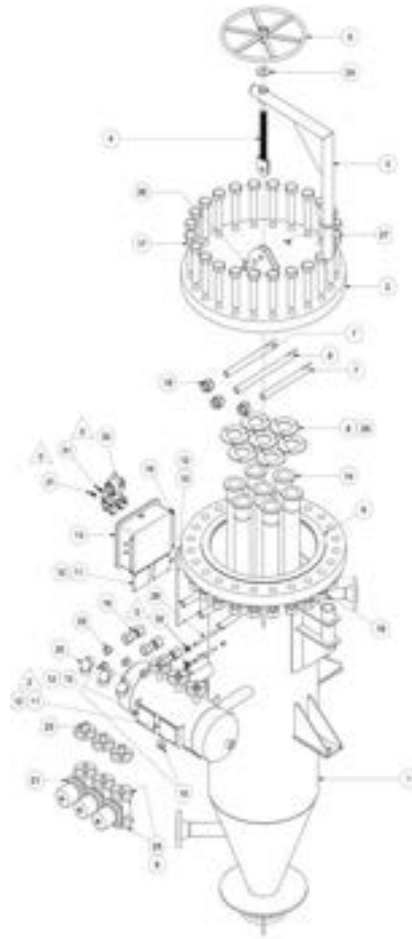
Figure 20. Secondary particle separator design.

For Operation 2, the back-pulse frequency was increased to 15 second intervals while maintaining solid circulation. Only electric gas heaters were engaged to heat process air and nitrogen sent into each reactor to prevent any moisture from entering the system. Figure 21(Top) illustrates the pressure build up across the filter. As shown, the pressure across the secondary particle separator continuously increased despite using a higher back-pulse frequency and preventing moisture from entering the filter.
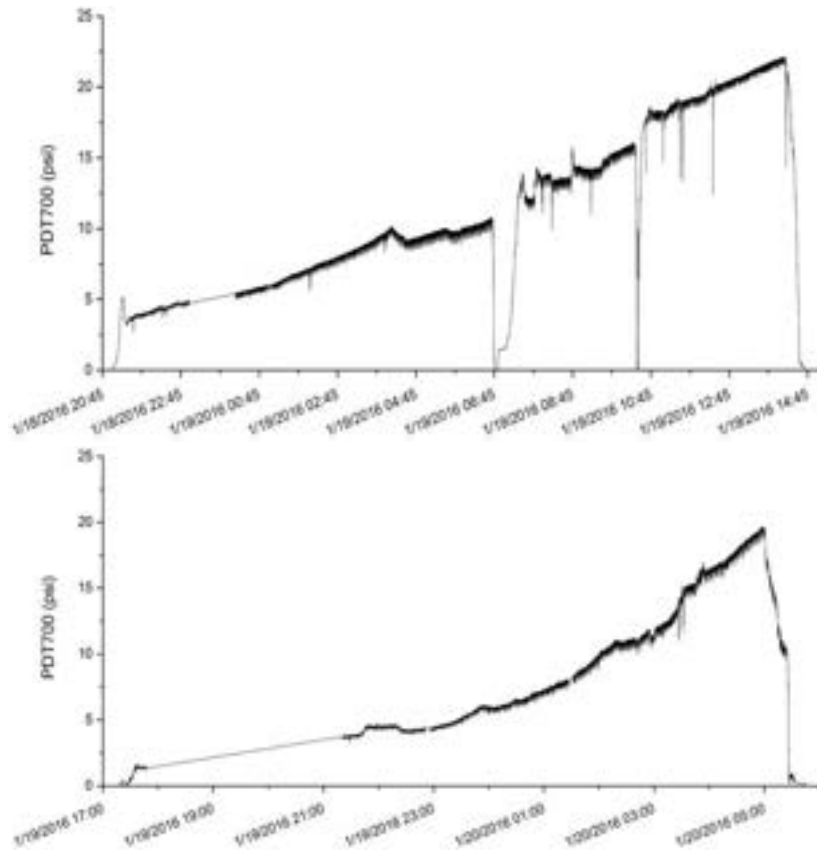
Figure 21. Pressure differential profile across secondary separator during Operation 2 (Top) and Operation 3 (Bottom)

Figure 22 shows the filter elements in the secondary particle separator after Operation 2. A layer of fines accumulated over the sinter metal filter elements was observed. No major fines accumulation was observed in the filter element housing. Also, the fines collected had no signs of moisture condensation which indicates the caking on the elements can occur even without moisture issues. Operation 2 was shut down due to pressure build up across the secondary particle separator.

Figure 22. Secondary particle separator filter elements after Operation 2.

Operation 3 was performed to verify the performance of the propane burner as well as to observe the performance of the secondary particle separator when the burner is in operation. Figure 21(Bottom) summarizes the pressure buildup profile across the secondary particle separator during Operation 3. Compared to Operation 2, the rate of pressure increase across the filter elements was much faster for Operation 3. Further, as shown in Figure 23, the layer of fines accumulated on the filter element after Operation 3 was greater than after Operation 2. After Operation 3, the solids discharge system downstream of the secondary particle separator was observed contain wet fines caked against the 2" reducing section connected to the filter element housing. The moisture collected on the fines is most likely due to the steam produced from propane combustion that condenses when reaching the secondary particle separator.

Figure 23. Image inside secondary particle separator after Operation 2.

During Operation 3, the performance of the added propane lances, reliable operation of the raw gas burner, and verification of all auxiliary gas heaters was tested successfully. However, major challenges still remained with operation of the secondary particle separator and fines discharge system. From the 3 operation runs, the issues discovered were:

1. Back-pulse system is unable to remove the fines collecting on the sinter metal filter elements

2. The gas temperature entering the secondary particle separator is below the dew point during burner startup resulting in moisture condensing on the filters and discharge piping

3. Fines are collecting in the 4" to 2" reducing union connecting the secondary particle separator to the discharge piping

4. Servicing secondary particle separator requires shutting down entire pilot system for 12 hours

Modifications were performed on the secondary particle separator and discharge system to address each issue observed during the startup operation. Specifically, as the operating temperature of the combustor flue gas entering the secondary particle separator will not exceed 500˚F, the sintered metal filters were replaced with fabric filters with a maximum operating temperature of 525˚F. Replacing the sinter metal filters with fabric filters reduced the cost of the overall system and simplified the back-pulse operation. To prevent moisture from collecting in the fines discharge system and secondary particle separator during startup, the gas and finds discharge piping were heat traced and insulated to maintain the flue gas temperature above its water dew point. The discharge system piping and valve components were enlarged from 2" to 4" pipe size to facilitate the free fall of fines through the lock hopper system and into the collection drum. Lastly, in case an issue is observed in the secondary particle separator and/or discharge system, a flue gas bypass system was added to allow the SCL pilot plant to continue operating while the equipment and components of the particle separator and discharge system are serviced. Figure 24 summarizes the modifications performed.

Original Design   **Modified Design**
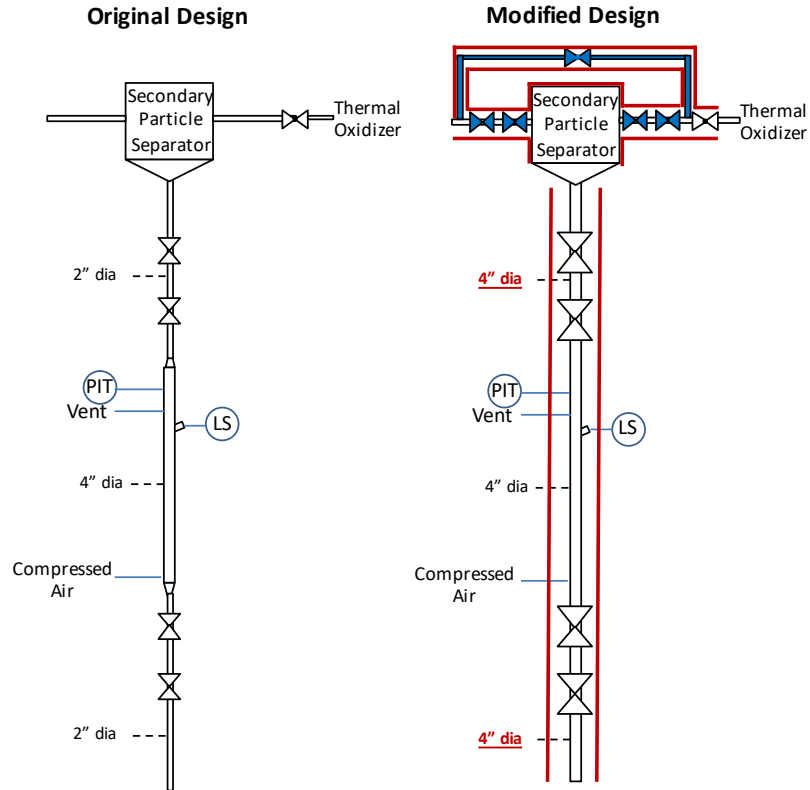
Figure 24. Simplified process flow diagram of the secondary particle separator and discharge system modifications performed to original design.

Fisher Klosterman redesigned the fabric filters and cages for assembly in the existing filter house, Nightwine valves provided 4" metal seated ball valves for the discharge system, and pipe fitters and electrical contractors installed the 4" piping and heat trace and insulation. Figure 24 are photos of the completed modifications. All components were installed and leak-checked.

Figure 25. Discharge modifications installed on site. (Top Left) 4" metal seated valve for lock hopper in discharge system; (Top Right) installed heat trace on piping; (Bottom) heat traced, insulated and installed bypass piping and control valve.

The fabric filters were installed and tested under ambient temperature and with solid circulation. Initial tests indicate the pressure across the filter elements did not increase. Figure 26 shows the photo of the fabric filter elements prior and after initial solid circulation tests. As illustrate, no major fines accumulation was observed on the elements. The heat tracing and ball valve operation on the secondary particle separator and discharge system were tested at the completion of the modifications.

Figure 26. Photo of fabric filter elements prior to (top) and after (bottom) initial solid circulation testing.

4.3.   Long-term testing and syngas injection

After completing the heat tracing of the secondary particle separator, heat tracing and enlarging the discharge system, and incorporating a bypass line around the secondary particle separator, process startup was performed again. The SCL pilot was first raised to 30 psig using N_2 to the combustor reactor. Once reached, air to the combustor was gradually increased until gas velocity exceeded minimum fluidization velocity. Aeration gas to the non-mechanical control valve was then initiated to commence solid circulation. Secondary particle separator back-pulse operation was set at 30 second intervals. The back pressure control valve on the combustor reactor and air flow rate were modulated to maintain proper system pressure and solids entrainment, respectively. N_2 to the reducer and oxidizer reactor were gradually started while modulating the reducer and oxidizer gas outlet control valves to account for the increased gas flow. Once solid circulation reached steady conditions, the electrical preheaters on the reducer, oxidizer, and combustor gas inlet were engaged with a temperature ramp rate of approximately 50°F/hour. Once the overall reactor temperature exceeded 250°F, the propane startup burner was initiated while maintaining 50°F/hour ramp rate for the gas temperature entering the combustor. On Day 5 of startup, system temperature of 1,600°F was reached. Figure 27 illustrates the temperature profile of the combustor exhaust gas throughout the temperature ramp up operation.
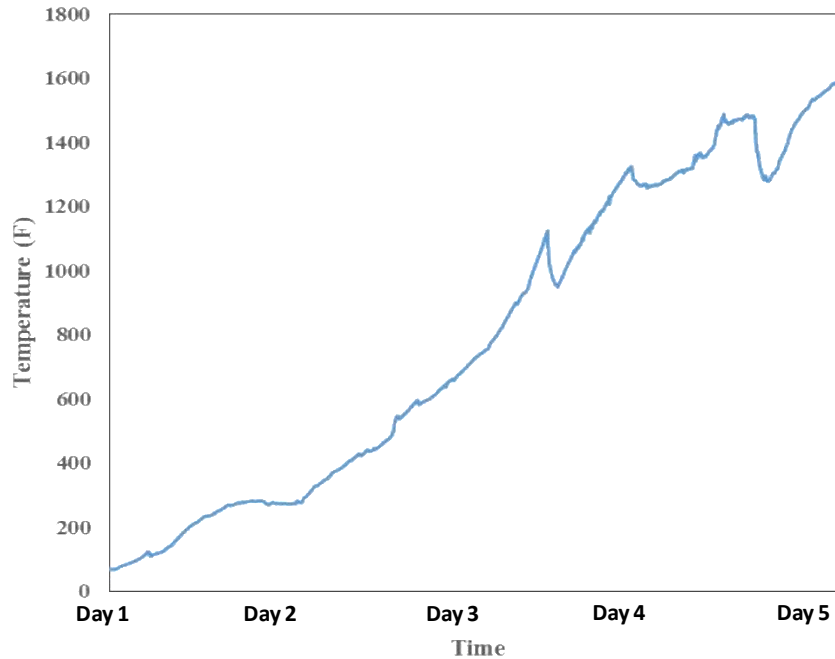
Figure 27. Temperature profile of combustor exhaust gas during SCL process heat up.

The reactor temperature rise was substantially lower than the ramp rate of the gas preheaters due to the large mass of insulating material in the reactor system. Additionally, as illustrated in Figure 27, several nuisance trips occurred during the system heat up due to faulty sensor measurements and minor compressor pressure control issues. The SCL system trips resulted in system depressurization and burner and burner shutdown. To recover from each system trip while preventing insulation damage, the system pressure was raised back to 30 psig while engaging the gas heaters with the initial setpoint temperature equal to the system temperature. The propane burner was also started immediately, after the trip, with the combustor air to prevent excessive cooling of combustor reactor and the windbox.

Compared to the original sinter metal filter elements, the GoreTex fabric filters allowed the back pulse system to function properly and no extended fines accumulation on the filters was observed as the differential pressure across the secondary particle separator was maintained steady throughout the system heat up. The differential pressure profile across the secondary particle separator during heat up is illustrated in Figure 28. Fines accumulation was also not observed in the discharge system.
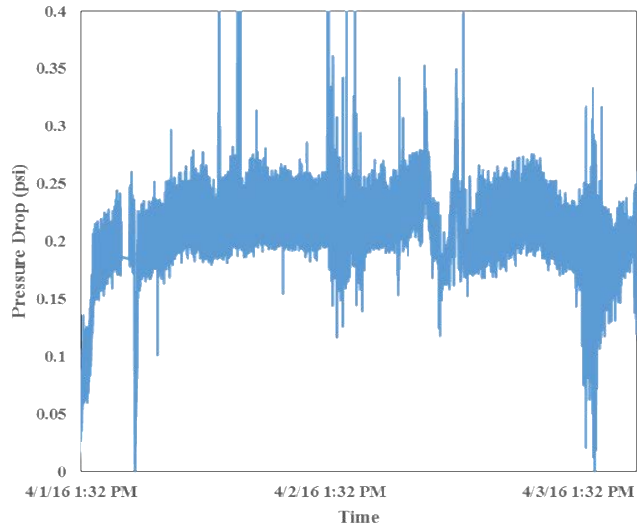
Figure 28. Sample differential pressure profile across secondary particle separator during system heat up.

Once 1,600°F was reached, the system pressure was raised to 60 psig and N2 was introduced to the zone sealing standpipes to generate gas sealing between the reducer, oxidizer, and combustor reactors. The gas analyzers on the reducer and oxidizer reactors were used to verify that no O2 was present in the reactors prior to the introduction of syngas to the reducer. The syngas supply piping was heated to 450°F using the installed mineral insulated heat tracing. To gradually replace the N2 gas injection to the reducer with syngas, the syngas inlet shutoff control valve was opened and the manual isolation valve for syngas line was gradually opened while gradually closing the manual isolation valve for the N2 supply. Once full transition to syngas was complete, the shutoff control valve for the N2 supply was commanded closed and the manual isolation valve was reopened. The gradual transition allowed the process to maintain gas sealing and proper solid circulation and to prevent system trips. Figure 29 illustrates the steady pressure profile in the reducer and oxidizer reactor during transition from N2 injection the reducer to syngas.
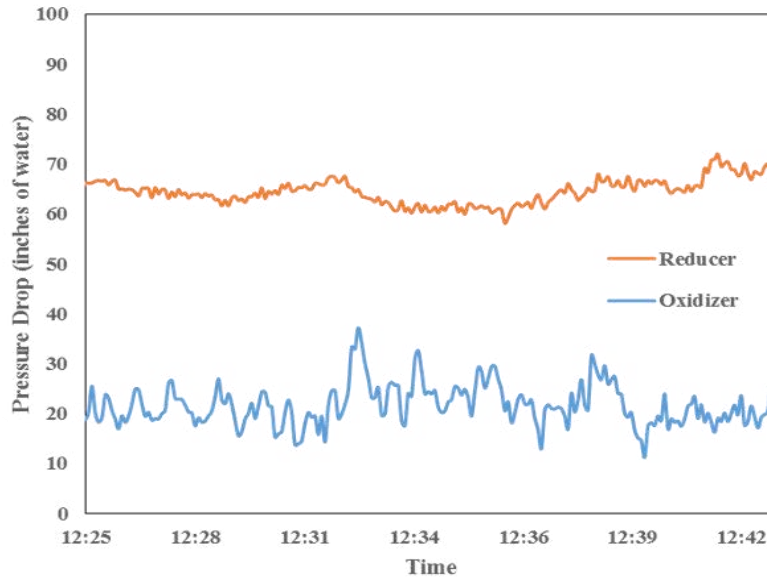
Figure 29. Differential pressure profile in reducer and oxidizer reactor during transition from N_2 injection to syngas in the reducer reactor.

During the initial syngas injection test, reducer outlet pressure gradually rose indicating an accumulation in the gas outlet piping preventing gas flow. Syngas injection was soon terminated replacing the reducer gas inlet flow with N2. Further analysis showed the gas temperature exiting the reducer gas outlet secondary cooler was approximately 125°F resulting in accumulation of condensed moisture in pipe line. To resolve this issue, cooling water to the secondary cooler was isolated and drained to bring the cooler offline. System trip interlocks were maintained to ensure the gas temperature did not exceed the maximum allowable working temperature of the pipe line (750°F). Once the cooler was brought offline, the reducer gas outlet temperature was raised to approximately 250°F and steady gas discharge was observed. Syngas injection was then re-established, and the reducer exhaust temperature was monitored to ensure it did not exceed 500°F. The syngas was introduced at 350 lb/hr during 10-hour operating period. Sample gas composition profile is illustrated in Figure 30. Steady syngas conversion of >98% was observed showing promising initial results for the SCL pilot. The oxygen carrier conversion was estimated to be 17%, which corresponded to an oxidation state of Fe3O4/FeO for the iron oxide and was already capable of converting steam to hydrogen.
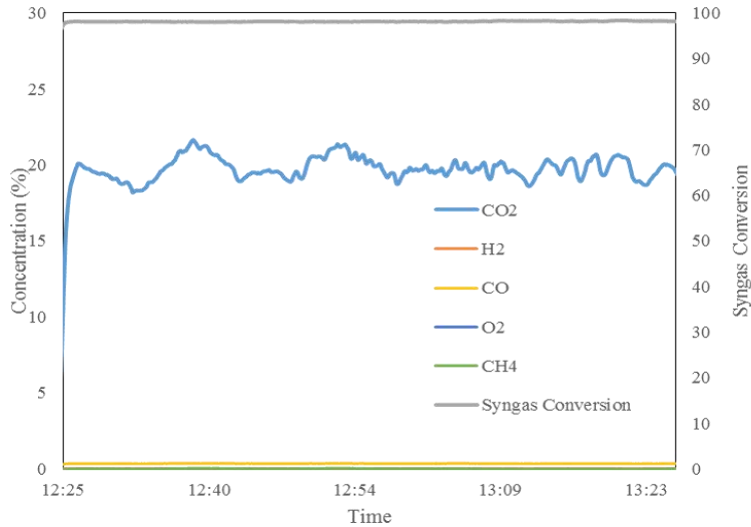
Figure 30. Sample reducer gas composition during syngas injection studies.

4.4.   Fluidization Troubleshooting

System shutdown was commenced due to an accumulation of debris observed in the upper zone seal standpipe. Once the process system was cooled the debris was removed from the standpipe and analyzed. The debris material was determined to be residual oxygen carrier fines accumulated along the reactor wall during initial testing in 2013 prior to full insulation dry out that sintered during dry out and detached during operation. The debris material was removed, and the system was further inspected for any issues prior to refilling the reactor with oxygen carrier particles to commence process startup. A second process startup operation was unsuccessfully completed due to damage observed in the combustor insulation. Further inspection and analysis were performed during the quarter to determine issue.

Combustor Inspection: During the second startup operation in Q2 2016, solid fluidization in the combustor could not be established preventing solid circulation from commencing. Systematic analysis of the combustor performance with gas flow was performed to understand the issue. Specifically, gas flow rates to the combustor were varied and the differential pressure value measured was compared to theoretically predicted values based on implicit correlation equations (i.e. Ergun's Equation) given the particle and gas characteristics. It was observed that the experimentally measured differential pressure measurement was 30% of the theoretically predicted value indicating gas channeling through the reactor may have been the cause of the solid fluidization issue. The combustor windbox was removed to inspect the combustor reactor.

OSU, B&W, NCCC, and Vesuvius reviewed the issue and determined the cause may be due to the dissimilar insulation materials resulting in a difference in thermal expansion during heating. To confirm the hypothesis, a hot gas flow test was conducted prior to removing the combustor. Oxygen carrier particles were discharged from the combustor reactor and loaded in the oxidizer reactor. Air was introduced through

the windbox at 700 lb/hr with the combustor gas outlet open. The oxygen carrier particles loaded in the oxidizer ensured the gas flow was directed through the combustor reactor. The air preheater HTR-200 was initiated and gradually ramped to 430°C. Conditions were held for approximately 6 hours. Every 30 minutes, the thermal imaging camera was used to examine the metal skin temperature around the combustor reactor and record abnormal temperature gradients. Local high skin temperature spots on the combustor reactor can indicate gas channeling through the back layer for the insulation compromising the performance of the thermal insulation barrier. Once complete, the reactor was cooled to room temperature and windbox removed to examine the insulation lining. The local high temperature points identified were approximately 15°C higher than the average surrounding skin temperature.

The inspection indicated 4 main defects in the combustor reactor that may allow for gas channeling through the insulation. To resolve this issue the combustor refectory must be repaired. Due to the small size of the combustor with multiple connecting nozzles, the removal of this reactor section from the vessel is required in order to properly perform the repair. To save on costs for an outside contractor, NCCC agreed to support the removal and reassembly of the combustor with support from B&W to design the rigging system and provide instructions for a safe removal of the reactor section. Louis Perry and Associates (LPA), the original civil engineer contractor for the project, was contracted by B&W to support the design rigging bars and calculations to ensure the temporary support structure can sustain the weight of the remaining reactor vessel during the relining period. Figure 31 shows the rigging design and removal instructions under review by NCCC.
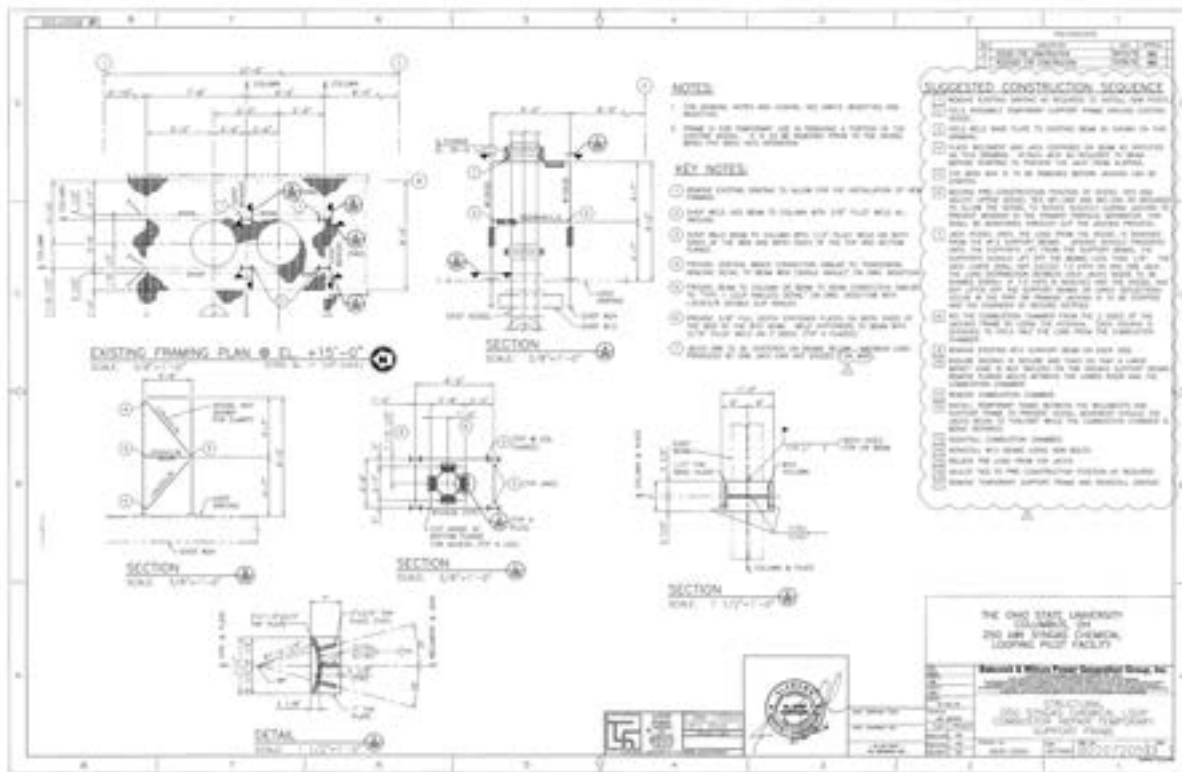
Figure 31. Combustor removal procedure and rigging design.

5. Long Term Test Campaign Two

5.1.   Pre-run preparation and pilot plant operation

The support frame designed was fabricated and assembled with the support from NCCC's Construction department. Mechanical jacks were set to supply appropriate force to counter the weight of the reactors above the combustor section. The pressure transmitters, particle makeup hopper, iso-kinetic device, propane injection lances and thermocouple inserts were removed and stored indoors. Gas tubing and piping were disconnected with the openings sealed to prevent dust and moisture from going into the system. The combustor vessel was successfully removed and shipped to Vesuvius for reinstalling the

insulation.   The   removal   process   is   shown   in

Figure 32. Then, the dry-out equipment was set up, and the 9-day slow dry-out procedure was completed in-house.
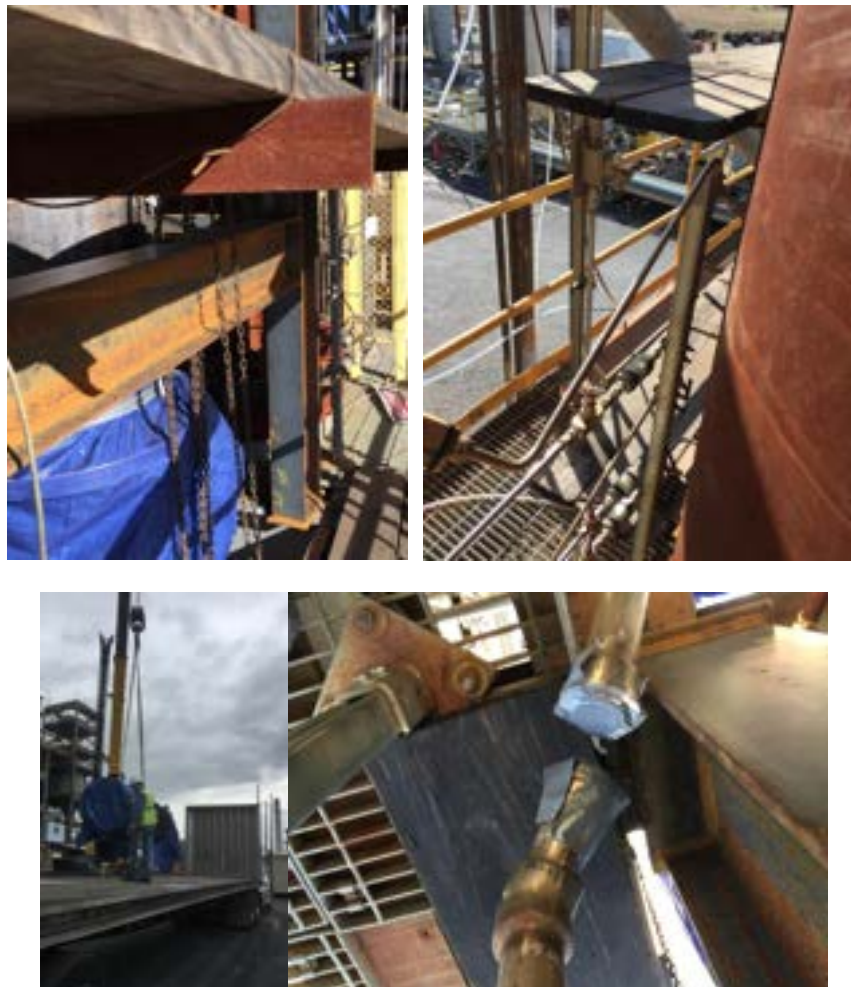
Figure 32. Combustor removal and reactor weather protection

5.2.   Repaired Combustor Testing

With the assistance from NCCC, the frustum combustor was removed from the SCL pilot unit and shipped to the insulation manufacturer, Vesuvius, for repairing. A 9-day slow dry-out procedure was completed in-house before the combustor was shipped back to NCCC. The relined combustor was installed back to the 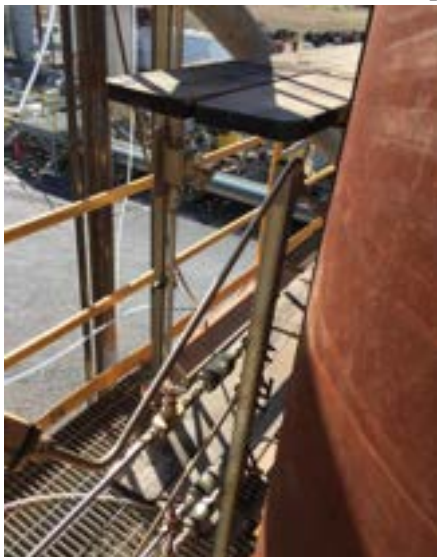SCL unit in April, 2017 and tested under cold flow condition. Figure 33 shows the combustor air flow rate and the corresponding pressure drop across the fluidized bed during the cold flow test. The pressure drop across the frustum combustor increased as the air flow rate through the combustor increased, which indicated that the gas bypassing was eliminated after the repair. The combustor was successfully fluidized by the air flow as verified by the fluctuation of pressure drop across the combustor.
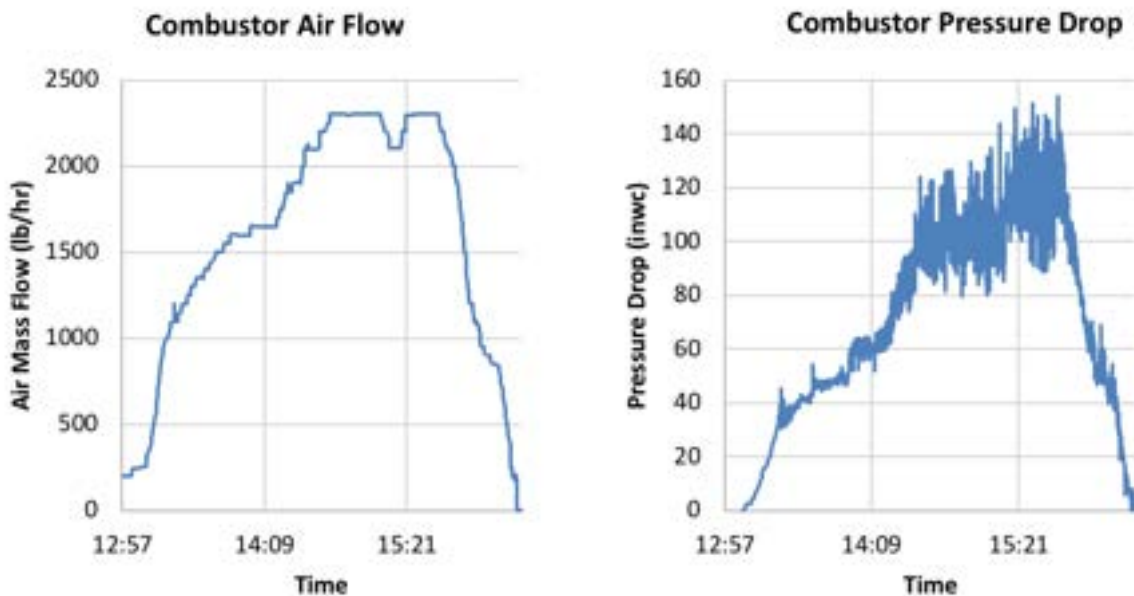
Figure 33. Combustor air flow rate and pressure drop during cold flow test.

5.3.   Hydrogen generation

Steam injection to the oxidizer was performed to validate the SCL process application to hydrogen production. Solid conversion before introducing steam was 25%. Using the same mass balance calculations performed on the reducer, the nitrogen-free gas yield from the oxidizer outlet can be obtained, as shown in Figure 34. When the steam was introduced, no syngas species was observed in the oxidizer, which indicated that the gas seal between the reducer and oxidizer was maintained. The H_2 molar flow rate plateaued at 60

mol/hr, while the molar flow rates of CO and CO_2 remained negligible. The result directly translates to >99% H_2 purity in the oxidizer product stream. Since no additional carbon species was generated in the oxidizer upon introducing stream, it also confirmed that no carbon deposition occurred in the reducer. The concept of SCL hydrogen production is thus verified, while further improvement of the performance can be expected with a higher solid conversion from the reducer and/or a non-diluted steam feed to the oxidizer.
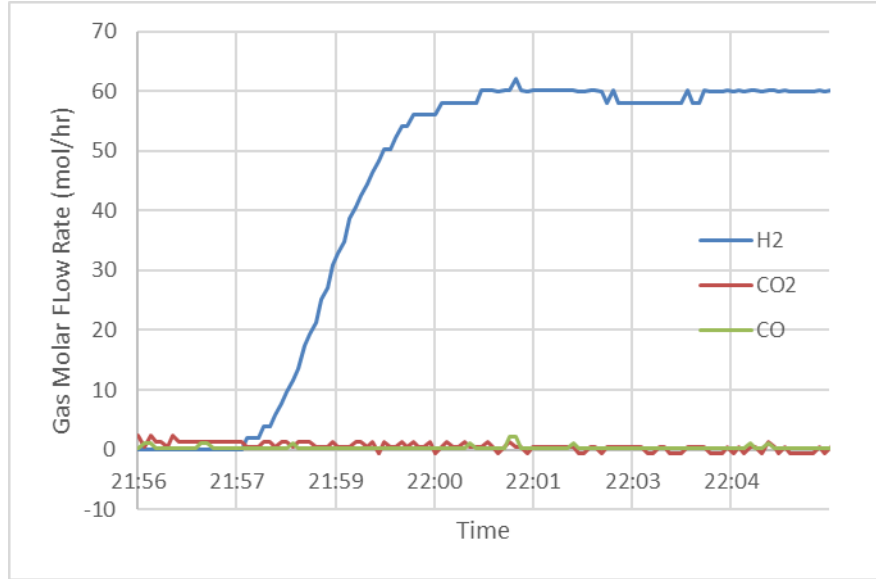
Figure 34. Molar flow rates of product gases in the oxidizer outlet stream during steam injection

5.4.   Post-operation data analysis

5.4.1 Product composition prediction using the ASPEN model

Three test conditions were demonstrated in the SCL pilot plant where the oxygen carrier to syngas feed ratio and reducer operating temperature were varied. Table 5 summarizes the three test conditions and the predicted gas and solid conversions calculated using the ASPEN simulation model described in Section 2.1. The oxygen carrier to syngas feed ratio, γ, is defined in Equation 4.

$$\gamma = \frac{\dot{m}_{Fe_2O_3}}{\dot{m}_{syn}} \qquad (4)$$

The individual conversions of the reducing gas species in the syngas fed into the reducer (i.e. H_2, CO and CH_4) and the overall syngas conversion are calculated from Equations 5 and 6.

$$X_j = 1 - \frac{\dot{n}_{k,out}}{\dot{n}_{k,in}} \quad (k = H_2, CO, CH_4) \qquad (5)$$

$$X_{syn} = \frac{\dot{n}_{CO,in} - \dot{n}_{CO,out} + \dot{n}_{CH4,in} - \dot{n}_{CH4,out} + \dot{n}_{H2,in} - \dot{n}_{H2,out}}{\dot{n}_{CO,in} + \dot{n}_{CH4,in} + \dot{n}_{H2,in}} = 1 - \frac{\dot{n}_{CO,out} + \dot{n}_{CH4,out} + \dot{n}_{H2,out}}{\dot{n}_{CO,in} + \dot{n}_{CH4,in} + \dot{n}_{H2,in}} \qquad (6)$$

As shown in Equation 7, the oxygen carrier conversion is defined as the extent of active lattice oxygen being transferred to convert the reducing gases in the syngas.

$$X_{OC} = \frac{3\,\dot{n}_{Fe_2O_3,out} + 4\,\dot{n}_{Fe_3O_4,out} + \dot{n}_{FeO,out}}{3\,\dot{n}_{Fe_2O_3,in}} \qquad (7)$$

Table 5. Summary of simulation predictions of gas and oxygen carrier conversions

	Condition 1	Condition 2	Condition 3
Temperature, °C	835	840	920
Fe_2O_3/Syngas mass ratio (γ)	2.319	0.575	0.575
CH_4 conversion (X_{CH_4})	100.00%	99.98%	100.00%
H_2 conversion (X_{H_2})	100.00%	55.78%	59.42%
CO conversion (X_{CO})	100.00%	22.30%	16.31%
Syngas conversion (X_{syn})	100.00%	41.40%	39.85%
Oxygen Carrier conversion (X_{OC})	17.34%	31.54%	30.66%

Condition 1 represents the operating condition with high oxygen carrier flow rate relative to the syngas feed. With sufficient lattice oxygen introduced to the reducer, the thermodynamic equilibrium favors complete conversion of the reducing gases to CO_2 and H_2O. The resulting X_{OC} is 17.34%, which corresponds to an oxygen carrier oxidation state between FeO and Fe_3O_4, favoring more towards Fe_3O_4. To explore the performance of the SCL reducer at higher X_{OC}, lower γ value is used in Condition 2 with similar operating temperature as Condition 1. The predicted X_{OC} calculated from ASPEN is 31.54%, resulting in FeO as the dominating oxidation state of the oxygen carrier. However, the high concentration of CO_2 and H_2O in the syngas stream fed into the reducer hinders the complete conversion of CO and H_2 at this γ value. The expected CO and H_2 conversion for Condition 2 is 22.30 and 55.78%, respectively. Condition 3 operates the reducer at a greater temperature, while maintaining the same γ as Condition 2. However, the model predicted results suggest that the CO and H_2 conversions are not very sensitive to temperature change within the temperature range of Conditions 2 and 3. Despite the insensitiveness of thermodynamic equilibrium to the reducer temperature, influence of temperature on the reaction kinetics is anticipated. The actual effect of temperature on the process is investigated in the experimental result discussion of Section 5.4.6.

5.4.2 Differential pressure of the reactors at steady state operation

The differential pressure across all the reactors was monitored during operation as an indication of stable gas and solid flow rates. Figure 35a and Figure 35b shows the typical differential pressures across the moving bed reducer (DP RDC), moving bed oxidizer (DP OXD), and fluidized bed combustor and entrained bed riser (DP CMB), during steady state operation. With the constant flow of gas across the moving bed reducer and oxidizer, the differential pressure measurements remained constant with minimal fluctuations. The fluidized bed combustor differential pressure measurements showed much greater fluctuations due to the slugging behavior of the large, Geldart Group D particles in this reactor. The 2-minute moving average of the combustor differential pressure, indicated by DP CMB_AVG in Figure 35 (b), shows the differential pressure in the combustor was approximately 60 inH₂O. Steady pressure measurements on the reducer, oxidizer and combustor reactors indicate the system is correctly designed and can be operated as intended.

(a)   (b)
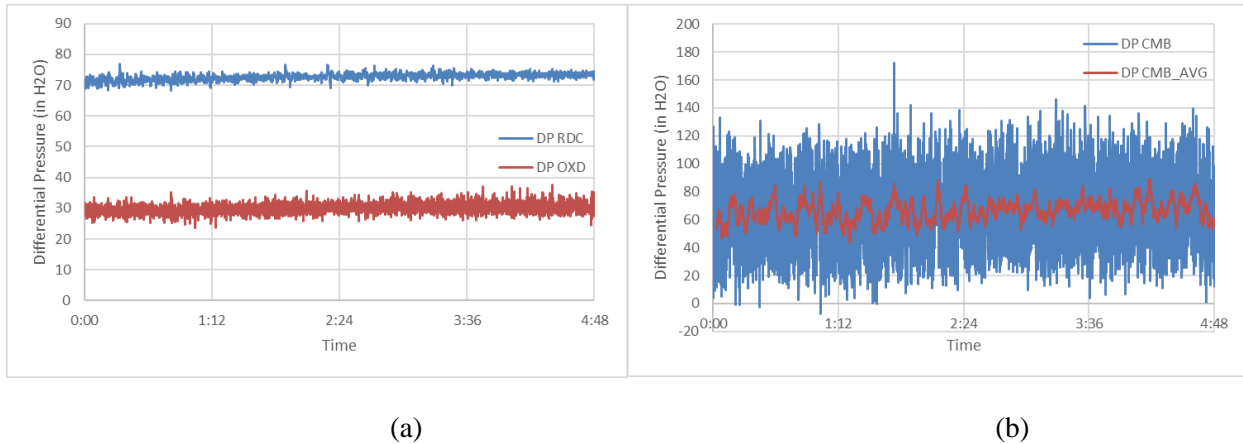
Figure 35. Steady-state differential pressures (DP) of (a) the reducer (RDC), oxidizer (OXD) and (b) combustor and riser combined (CMB)

5.4.3 Experimental result evaluation

To evaluate the performance of the SCL process during the testing, the gas concentrations analyzed from the reducer gas inlet and outlet are used to calculate the syngas and oxygen carrier conversions. Based on the syngas mass flow rate, $\dot{m}_{syn}$, measured by the flow meter placed on stream 1 in Figure 3, the molar flow rate of the syngas $\dot{n}_{syn}$ can be obtained from Equation 8:

$$\dot{n}_{syn} = \frac{\dot{m}_{syn}}{\sum_i M_i \cdot C_{i,in}} \qquad (8)$$

where M_i and $C_{i,in}$ are the molecular weight and molar concentration of each gas species i (N_2, O_2, H_2, H_2O, CO, CO_2, CH_4). Subsequently, the molar flow rate of each species going into the reducer, $\dot{n}_{i,in}$, is calculated from Equation 9:

$$\dot{n}_{i,in} = \dot{n}_{syn} \cdot C_{i,in} \qquad (9)$$

The source of the syngas is an air-blown, transport gasifier, where the nitrogen concentration in the syngas stream is approximately 70%. The nitrogen in the syngas does not react with the oxygen carrier in the reducer. Therefore, it can be used as a tracer gas to determine the molar flow rate of each gas species exiting the reducer, $\dot{n}_{j,out}$, as defined in Equation 10:

$$\dot{n}_{j,out} = \frac{\dot{n}_{N_2}}{1 - \sum_j C_{j,out}} \cdot C_{j,out} \qquad (10)$$

where j represents the species directly measurable by the gas analyzers, including O_2, H_2, CO, CO_2 and CH_4. Based on the definitions described in Section 3.1, the individual conversions of H_2, CO and CH_4, and the overall syngas conversion during operation can be calculated.

The molar flowrates of all the major species which contain oxygen atom are measured by the gas analyzer, except for the condensed H_2O at the outlet. The molar flow rate of H_2O can be calculated by hydrogen balance as defined in Equation 11:

$$\dot{n}_{H_2O,out} = 2\left(\dot{n}_{CH_4,in} - \dot{n}_{CH_4,out}\right) + \left(\dot{n}_{H_2,in} - \dot{n}_{H_2,out}\right) - \dot{n}_{H_2O,in} \qquad (11)$$

assuming the hydrogen is only converted to no species other than H_2, H_2O and CH_4 at the outlet. The oxygen carrier conversion in the reducer can be obtained by comparing the rate of oxygen transferred into the gas phase with the flow of lattice oxygen available in Fe_2O_3, as shown in Equation (12):

$$X_{OC} = \frac{2\left(\dot{n}_{CO_2,out} - \dot{n}_{CO_2,in}\right) + 2\left(\dot{n}_{O_2,out} - \dot{n}_{O_2,in}\right) + \left(\dot{n}_{H_2O,out} - \dot{n}_{H_2O,out}\right) + \left(\dot{n}_{CO,out} - \dot{n}_{CO,in}\right)}{\dot{m}_{Fe_2O_3} \cdot \frac{3}{M_{Fe_2O_3}} \cdot 1000} \qquad (12)$$

where $\dot{m}_{Fe_2O_3}$ represents the mass flow rate (kg/hr) of iron oxide in the form of oxygen carrier particles, measured by the isokinetic device.

5.4.4 Syngas and Oxygen Carrier Conversion

Figure 36 shows the steady-state gas concentration profiles recorded at the reducer inlet and outlet during the syngas injection period under Condition 1. The syngas flow rate was maintained at 158.76 kg/hr, which corresponded to 120 kW$_{th}$ plant capacity. The oxygen carrier particles were introduced to the reducer at around 835°C with $\dot{m}_{Fe_2O_3}$ of 368.20 kg/hr. The product gas mainly consisted of ~20% CO_2, ~0.35% CO, and balanced nitrogen. Negligible H_2, O_2 and CH_4 were detected, indicating high conversion of these species.

(a)   (b)
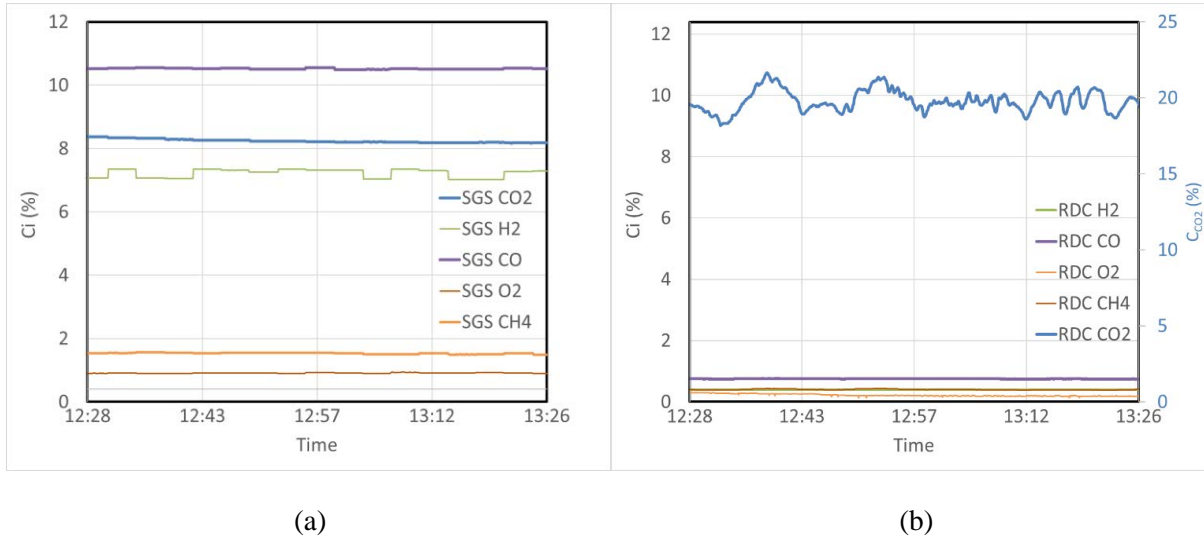
Figure 36. Steady-state gas concentration recorded at the reducer (a) inlet and (b) outlet during the syngas injection period under Condition 1

A carbon balance was done based on the molar flow rates of C species at the inlet and outlet of the reducer, as shown in Figure 37. The carbon balance was found to close with an average deviation of 4%. The deviations were attributed to the semi-batch feed of coal in to the gasifier, which caused the syngas concentration to vary over time. Hence, the gas conversions can be reliably calculated using Equation 5 and 6.
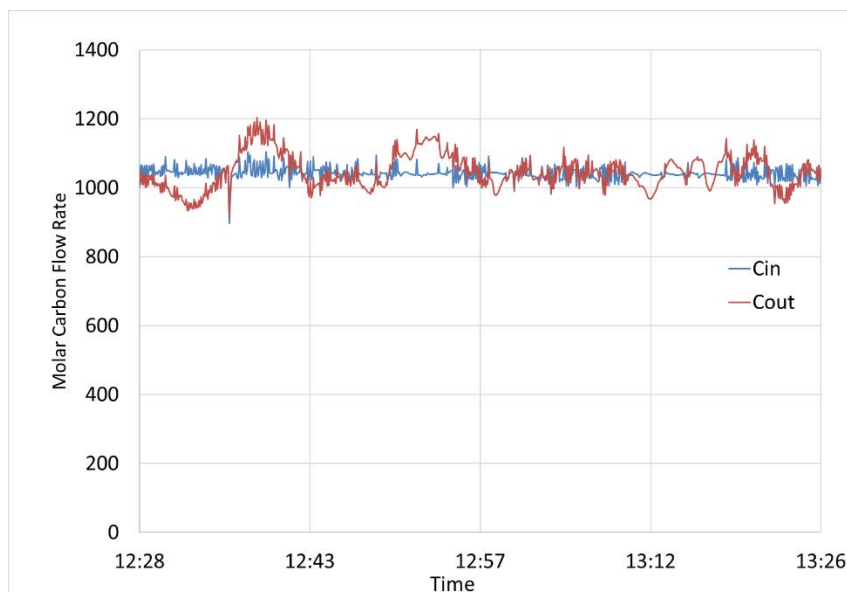
Figure 37. Calculated carbon molar flow rates at the reducer inlet and outlet under Condition 1

From the concentration measurements, the corresponding conversions of the reducing gas species, i.e. H_2, CO, CH_4, were calculated using equation (8) and are shown in Figure 38. A 100% conversion of H_2 was maintained while CH_4 and CO conversions were slightly less than 100% owing to their relatively slower reaction rates compared to H_2.[33] The CO conversion was 96.8%, whereas the CH_4 conversion fluctuated between 93.6% to 98.5%. The syngas conversion, calculated using Equation 9, was roughly around 98%, which proves the excellent performance of a moving bed reducer and successful scale-up in a pilot plant.
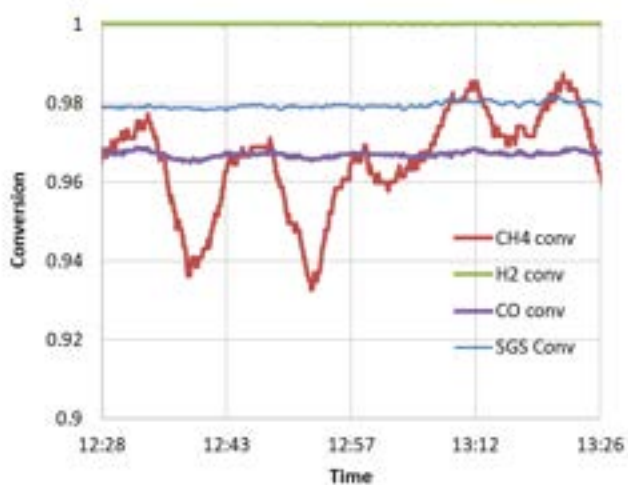
Figure 38. Gas conversions in the reducer under Condition 1

From the measured gas flow rates and concentration, the oxygen carrier conversion was calculated and shown in Figure 39. The average oxygen carrier conversion was around 16.5%. As discussed in the Introduction, oxygen carrier conversion greater than 11% indicates a mixture of FeO and Fe_3O_4. This result demonstrates that oxygen carrier conversion greater than those achieved in fluidized bed can be obtained for a nearly complete gas conversion, which also allows for H_2 generation from steam in the oxidizer.
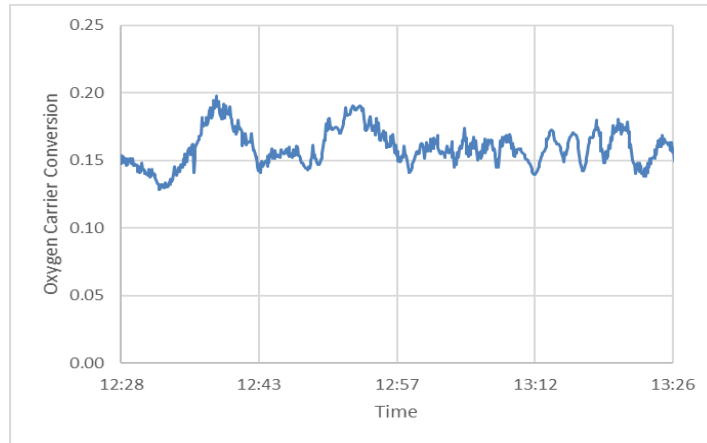
Figure 39. Calculated oxygen carrier conversion under Condition 1

Table 6 shows a comparison of the experimental result and ASPEN mode. The conversions of the reducing gases and oxygen carrier from the experimental data (Exp 1) were all very close to the values predicted by ASPEN (Sim 1), which indicates that the reaction kinetics was sufficiently fast to reach thermodynamic equilibrium.

Table 6. Comparison of gas and oxygen carrier conversions from experiment and simulation under Condition 1

	Condition 1	
Temperature (°C)	835	
	Exp 1	Sim 1
Fe_2O_3/Syngas mass ratio (γ)	2.319	2.319
CH_4 conversion (X_{CH_4})	96.02%	100.00%
H_2 conversion (X_{H_2})	100.00%	100.00%
CO conversion (X_{CO})	96.71%	100.00%
Syngas conversion (X_{syn})	97.95%	100.00%
Oxygen Carrier conversion (X_{OC})	16.03%	17.34%

5.4.5 CH4 reaction kinetics

The experimental results of Condition 2 are shown in Table 7. The reducer temperature was at 840°C. The particle circulation rate was decreased to around 104.33 kg/hr by lowering the L-valve nitrogen flow rate, while the syngas flow rate was increased to 181.44 kg/hr. Thermodynamically speaking, the oxygen carrier conversion should reach the maximum value of 31.54%, as shown in in Sim 2a in Table 7. The oxygen carrier conversion was calculated to be 32%, which was in good agreement with the prediction. Every reducing gas conversion, however, showed more than 20% of discrepancy between Exp 2 and Sim 2. The mismatches were attributed to the inaccurate prediction of CH_4 conversion in ASPEN simulation, which had no information regarding reaction kinetics and assumed full conversion of CH_4. In reality, only 20% of the CH_4 was converted, and most of the lattice oxygen transferred from the oxygen carriers was used to convert H_2 and CO to H_2O and CO_2, thus the H_2 and CO conversions were higher than expected. To account for the reaction kinetics of CH_4, another set of simulation was performed with 80% of CH_4 manually bypassed the reducer model, as shown in Sim 2b. The adjustment effectively narrowed all the gas conversion discrepancies to less than 7.5% while affecting little on the oxygen carrier conversion.

Table 7. Comparison of gas and oxygen carrier conversions from experiment and simulation under Condition 2

	Condition 2		
Temperature (°C)	840		
	Exp 2	Sim 2	Sim 2b
Fe₂O₃/Syngas mass ratio (γ)	0.575	0.575	0.575
CH₄ bypass	N/A	0	80%
CH₄ conversion (X_{CH_4})	19.96%	99.98%	20.00%
H₂ conversion (X_{H_2})	79.21%	55.78%	72.24%
CO conversion (X_{CO})	49.77%	22.30%	42.41%
Syngas conversion (X_{syn})	61.05%	41.40%	53.50%
Oxygen Carrier conversion (X_{OC})	32.05%	31.54%	29.60%

5.4.6 Temperature effect

To investigate the temperature effect, the reducer temperature was ramped up by using a higher burner capacity. The transient results during the ramping period are shown in Figure 40 and Figure 41. With the temperature risen from 840 to 920°C (Table 8, Condition 3), the syngas conversion also gradually increased to 70%. The maximum oxygen carrier conversion reached 45% which corresponds to an oxidation state of Fe/FeO for the oxygen carrier. Compared to the experimental results (Exp 3a), none of the conversion values matched the simulation (Sim 3a). Not only the gas conversions showed more than 25% discrepancies, the calculated oxygen carrier conversion was also 14.4% higher than the prediction value.

Using the same rationale as discussed in Section 3.4 regarding CH_4 reaction kinetics, 70% CH_4 bypass was implemented to generate Sim 3b. Despite the CH_4 bypass adjustment, the gas conversions in Exp 3a and Sim 3b were still more than 14% apart, while the difference between the oxygen carrier conversions increased to 15.4%, indicating that the CH_4 reaction kinetics was not the only reason for the discrepancy.

The two other factors affecting gas and oxygen carrier conversion were investigated, i.e γ and temperature. The effect of these two factors on gas and oxygen carrier conversion was explored using a sensitivity analysis in the ASPEN model of the reducer. Figure 42 shows the results of the sensitivity analysis in a 3-dimentional plot where γ is the main factor influencing the reducer performance. The effect of γ is represented in detail under a fixed temperature of 920°C in Figure 43. It is observed that the gas conversions for a higher γ of 0.8 predicted by the model (Sim 3c) better matches the experimental values compared to the ones of 0.575. Since the syngas flow rate did not change during the experiment, a higher value of γ would result from a higher solids circulation rate than was calculated originally, i.e. the actual Fe_2O_3 mass flow rate could be faster than 104.33 kg/hr. A γ value of 0.8 corresponds to a higher Fe_2O_3 mass flow rate of 145.15 kg/hr, which is then used to recalculate X_{OC} by Equation 15. As shown in Exp 3b, the recalculated X_{OC} is 32.35% and matches closely to the value of 29.60% in Sim 3c. The matching results of Exp 3b and Sim 3c suggest that the circulation rate may have accelerated over the course of temperature ramp. Possible explanation could be that the mass flow rate of the L-valve aeration gas was not adjusted during the temperature ramp, thus the solid circulation rate could have deviated from flow rate measured previously. As gas density decreases when the temperature increases, the linear velocity of the aeration gas theoretically increases, which leads to acceleration of the solid flow at the L-valve.
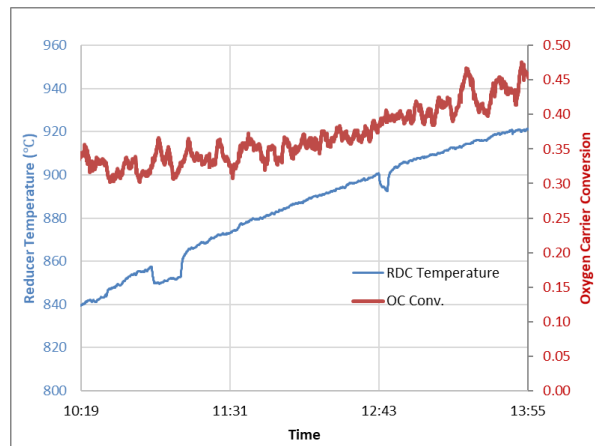
Figure 40. Transient profiles of reducer temperature and calculated oxygen carrier conversion from Condition 2 to Condition 3
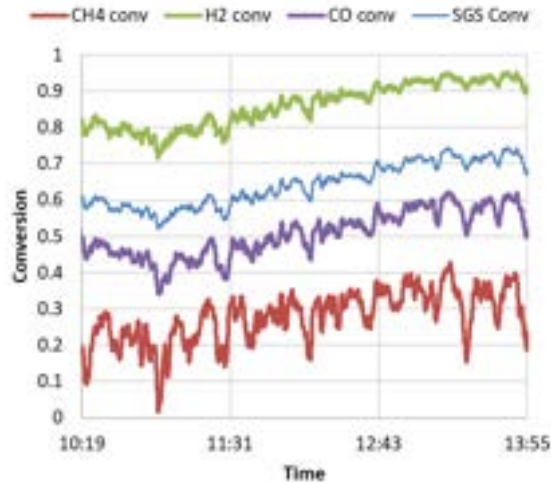
Figure 41. Transient gas conversion profiles from Condition 2 to Condition 3

Table 8. Comparison of gas and oxygen carrier conversions from experiment and simulation under Condition 3

	Condition 3				
Temperature (^oC)	920				
	Exp 3a	Exp 3b	Sim 3a	Sim 3b	Sim 3c
Fe_2O_3/Syngas mass ratio (γ)	0.575	0.8	0.575	0.575	0.8
CH_4 bypass	N/A	N/A	0	70%	70%
CH_4 conversion (X_{CH_4})	29.49%	29.49%	100.00%	30.00%	30.00%
H_2 conversion (X_{H_2})	90.77%	90.77%	59.42%	73.69%	86.45%
CO conversion (X_{CO})	58.66%	58.66%	16.31%	36.20%	65.73%
Syngas conversion (X_{syn})	65.75%	65.75%	39.85%	51.56%	72.13%
Oxygen Carrier conversion (X_{OC})	45.01%	32.35%	30.66%	29.60%	29.60%
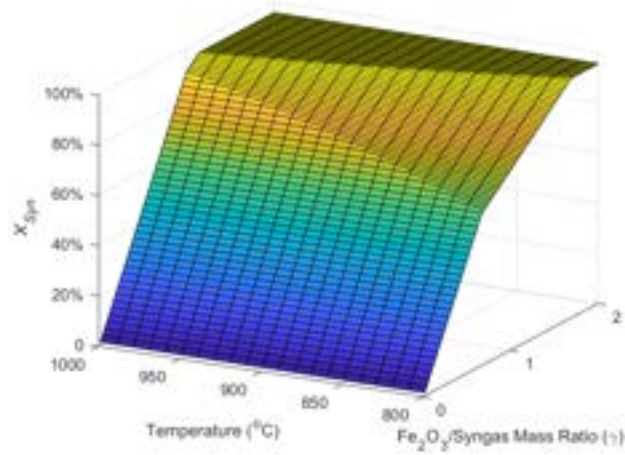
Figure 42. Sensitivity analysis of temperature and γ on syngas conversion under with methane conversion set at 30%
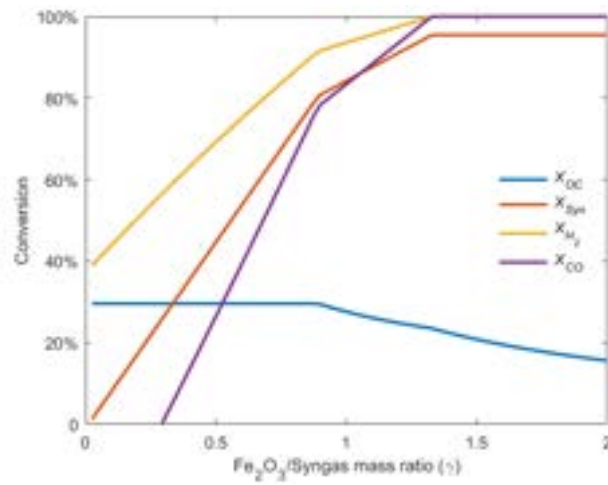
Figure 43. Parametric study of γ's effect on syngas conversion with methane conversion set at 30% and temperature at 920°C

6. Market/Deployment Assessment Activities

6.1.   Update CTL with SCL H$_2$ production economic model

The SCL system in this analysis processes a mixture of Fischer-Tropsch tail gas and clean syngas. The baseline plant uses ~5000 tonne per day of bituminous coal to produce syngas using oxygen from an air separation unit. The syngas is shifted and cleaned using a Selexol sulfur removal system before being sent to Fischer-Tropsch reactor system for producing higher hydrocarbons. The baseline chemical looping system uses tail gas to enhance the H$_2$ production. This higher H$_2$ production results in a higher per pass conversion to the FT system (75% vs 50%) and results in 19% less carbon emissions for the chemical looping system. The chemical looping system is assumed to cost ~16.15 million for a volume of 180m^3. The fuel reactor was sized to be 216 m^3 (cost of \$18million), oxidizer was sized to be 180 m^3 (cost of 16.12 million), the riser and the cyclone were sized to be ~4.8 million resulting in a total of 38.91 million \$'s (2000 dollars).

The addition of chemical looping allows for the expensive Selexol to be replaced by a cheaper MDEA and a sulfur guard system as per the calculations are shown in Table 9. Further, CO$_2$ compression and FT recycle compression cost significantly reduced resulting in an overall reduction in capital cost. The NCCC SCL operation was used to verify the assumed chemical looping reactor costs and the contingencies associated with them. For the same capital and operating cost investment, SCL system results in a 10% increase in liquid fuel yield. Task 6.2 provides a cost estimate based on the SCL pilot plant operation at the NCCC of \$ 934,000 for 5 m^3 of the chemical looping system (2011 dollars). This cost estimate is scaled to the size evaluated in the coal to liquids report, using a factor of 0.7 and a Marshall and Swift Index based adjustment resulting in a reducer cost of \$13 million for the fuel reactor, \$11 million for the oxidizer and a total reactor cost of \$30 million.[1] This cost estimate validates the conclusions of the original study which shows that adopting an SCL system in Coal to Liquids Fischer Tropsch plant results in higher cost savings from an operating cost perspective and a capital cost perspective as highlighted by the sensitivity study in Figure 44.

---

[1] Assessment, Independent, and Fischer-Tropsch Plant. "Chemical-Looping Process in a Coal-to-Liquids Configuration." (2007) DOE/NETL-2008/1307
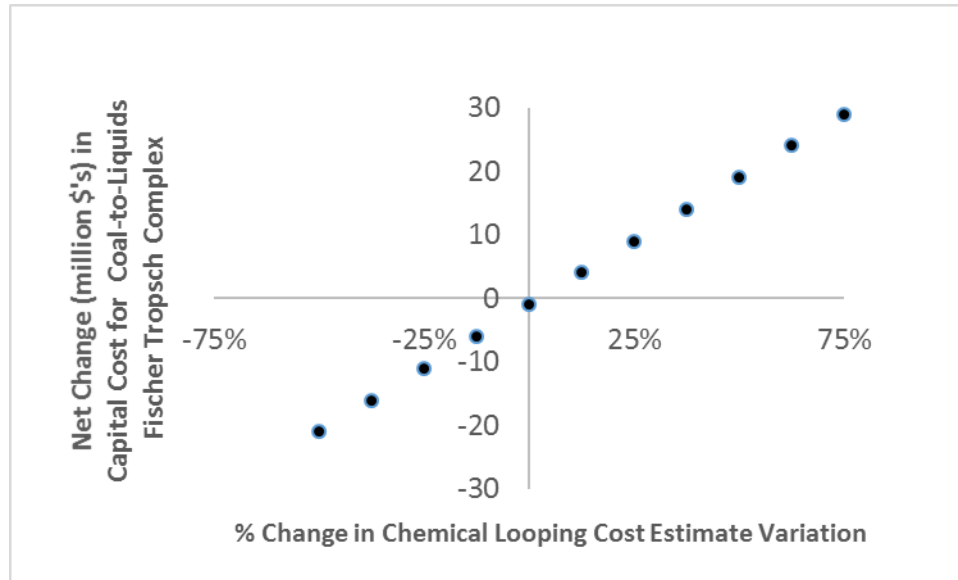
Figure 44. Sensitivity of the variation of the chemical looping capital cost estimate to the net change in the total cost of the FT plant

Table 9. Cost adjustment comparisons for applying the SCL chemical looping system to an FT plant

Item	Incremental Cost (MM$)
Add Looping System (OSU Estimate)	40
Eliminate Shift	-15
Eliminate Two Stage Selexol	-65
Add single stage MDEA and polisher	40
Increase F-T Reactor Size	5
Eliminate F-T Recycle	-8
Reduce CO_2 Compression Cost	-8
Improved Heat Exchanger Metallurgy	10
Net Change	-1

6.2.   Analyze reactor capital cost dependence on scaling

An updated simulation was performed based on the pilot scale demonstration parameters like the relevant syngas, steam and air preheat temperatures and solids circulation rates. In addition to updating the base process simulation model, sensitivity analysis on the maximum reducer outlet temperature, the amount of weight support for the solids in the reactor and variations in steam conversion were completed. These sensitivity studies are summarized as four cases with the relevant operating conditions as given in Table 10:

Table 10. Sensitivity analyses of relevant operating conditions

Case Number	% weight support for iron-oxide particles	Design temperature for the reducer inlet reactor (ºC)	Reducer reactor outlet temperature (ºC)	Oxidizer Reactor outlet temperature (ºC)	Design steam conversion in the oxidizer reactor
1	60	1000	750	795	42%
2	60	950	722	757	50%
3	50	1000	700	750	45%
4	50	950	690	740	56%

The simulation was used in conjunction with the actual pilot plant data to confirm and verify broad applicability of the SCL reactor cost. Overall, the SCL pilot scale reactors cost $930,000 for a reactor volume of 1 m^3, including the cost for construction, installation, project management and labor cost associated with the NCCC unit. This cost estimate is used as the basis for validating costs in Task 6.1 and used in Task 6.4 for discussions with industrial evaluators and partners.

6.3.   Develop SCL-IGCC economic model

The flow diagram of the SCL process used for evaluation in an IGCC application is given in Figure 45. The SCL process cogenerates hydrogen and electricity from coal-derived syngas via cyclic reduction and oxidation of specially-tailored iron oxide composite particles. The SCL process adopts the countercurrent moving bed reactor design for both the reducer and the oxidizer, where a concentrated carbon dioxide stream and a pure hydrogen stream are separately produced. The high-temperature flue gas from the combustor can be used for electricity generation. The SCL process in an IGCC application for hydrogen production consists of the following major units or systems: a Shell gasifier, an ASU, a gas quenching loop, a warm gas clean-up unit, the chemical looping reactor system, HRSG unit, and pressure changers.

Figure 45. Process flow diagram of Syngas Chemical Looping process

In this process, coal is first pulverized and dried. The coal powder is then pressurized in the lock hopper and introduced to the Shell gasifier for partial oxidation at 1,400°C and 30 atm. The high-temperature raw syngas from the gasifier is quenched to ~950°C with low temperature syngas. The quenched syngas is further cooled down to 550°C before entering a hot gas cleanup unit, which reduces the sulfur content in the syngas below 100 ppm. The low sulfur syngas is fed to the SCL reactor system for hydrogen production. The oxygen carrier conversion in the reducer is assumed to be 50%, and the steam to hydrogen conversion is assumed to be 60%. Also, 10% excess air is used in the combustor. The oxygen carrier contains 70% Fe_2O_3 by weight balanced with inert support. The corresponding solids circulation rate in a 1000 MW_{th} commercial plant is 1,551 ton/hour. In the current simulation, the reducer is operated at 900 °C and 31 atm, the oxidizer operates at 790°C and 31 atm, and the combustor is operated at the same pressure as the oxidizer with an operating temperature of 1050°C. All three reactors are operated at near adiabatic conditions.

Steam-iron reaction takes place in the oxidizer for hydrogen production. 249.4 ton/hour of medium pressure steam is injected to the oxidizer at about 300 °C. The flow rate of the compressed air to the oxidizer is 173.1 tons/hour. Three hot gas streams i.e., concentrated H_2O/CO_2 stream from the reducer, H_2O/H_2 stream from the oxidizer, and the exhaust gas stream from the combustor, is produced from the SCL reactors. Heat is extracted from both the reducer and oxidizer product gas streams for steam generation. During heat extraction, the steam in the product gas streams condenses out, resulting in high purity CO_2 and H_2 streams. 90% of the CO_2 rich stream from the reducer is sequestered after steam condensation. The exhaust gas from the combustor enters the HRSG section where it is cooled to 500°C and then filtered and expanded to ambient pressure. The steam conditions in the HRSG are 12.4 MPa/566°C/566°C. In order to superheat the pressurized steam, an additional firing section is installed in the HRSG to combust tail gas and hydrogen fuel at ambient pressure. A high-temperature gas turbine is not used in order to reduce the cost of the hydrogen plant.

Based on the parameters and process configurations described above, process simulation and economic analyses are conducted. For comparison, the conventional coal to hydrogen process with a hot gas cleanup unit is analyzed as a baseline case. The key techno-economic analysis results for both processes

operated under standard conditions are summarized in Table 11. From a process efficiency standpoint; the SCL process has a higher thermal efficiency for hydrogen production than the conventional coal to hydrogen process. The SCL process can produce 16.02 tons/hr of hydrogen with 90% CO_2 capture. Meanwhile, 25.2 MW of net electricity can be generated. The overall process efficiency from coal to hydrogen and electricity is 65.7%, which is considerably higher than the conventional coal to hydrogen process. For the economic analysis, an equivalent Levelized cost of electricity (LCOE) is estimated by converting hydrogen to electricity equivalent by multiplying the hydrogen production rate (in MW_{th}, HHV basis) with a factor of 0.6. The equivalent LCOE for the SCL process is nearly 10% lower than that for the baseline gasification process.

Table 11. Comparison of the Process Analysis Results

	Baseline	SCL
Coal Feed (tonnes/hour)	132.9	132.9
Carbon Capture (%)	90	90
Net Electricity (MW)	0.1	25.2
Hydrogen Product (tonne/hr)	15.28	16.02
Efficiency (%)	60.2	65.7
Total Plant Cost ($Million)	822.3	801.6
Equivalent LCOE ($/MWh)	110.0	100.7

The results for the study above are promising with the assumption of an oxygen carrier composition that is 70wt% Fe_2O_3 balanced with inert support. The NCCC sub pilot scale operation was operated to verify the assumptions on the pressure drops for reactor design, particle operating cost and reactor sizes. An adiabatic simulation model was developed to quantify the changes that occur in the assumed reducer performance with a lower active Fe_2O_3 wt%. The critical parameters which affect the Hydrogen production and ultimately the plant efficiency and cost are the temperatures for reducer operation and solids conversion. Figure 46 shows the comparison for solids outlet temperature and flowrate form the reducer reactor for the same fuel capacity. Figure 46 shows that as the active content of Fe_2O_3 is decreased, solids conversion from the reducer outlet is increased as more lattice oxygen is abstracted by the reducing fuel gas per unit amount of Fe in the system. This is crucial as it provides for a higher degree of H_2 production from the oxidizer, which is thermodynamically impossible from the 70wt% Fe_2O_3. Another parameter that was analyzed is the comparison of reducer outlet temperature under adiabatic conditions for varying Fe_2O_3 wt% as shown in Figure 47. The decrease of Fe_2O_3 wt% leads to an increase in inert support % and for the same fuel processing capacity results in a higher reducer outlet temperature. This has the advantage of obtaining faster kinetics and leading to a smaller reactor size. The simulation results from Figure 46 and

Figure 47 show an equivalent or better performance when used with a lower Fe_2O_3 wt% which was used in the SCL pilot scale demonstration. This indicates that the assumption of 70wt% Fe_2O_3 that yields a reduction in the cost of electricity as shown in Table 11 is a conservative assumption and the performance based on that assumption is achievable based on pilot scale testing of the SCL process.
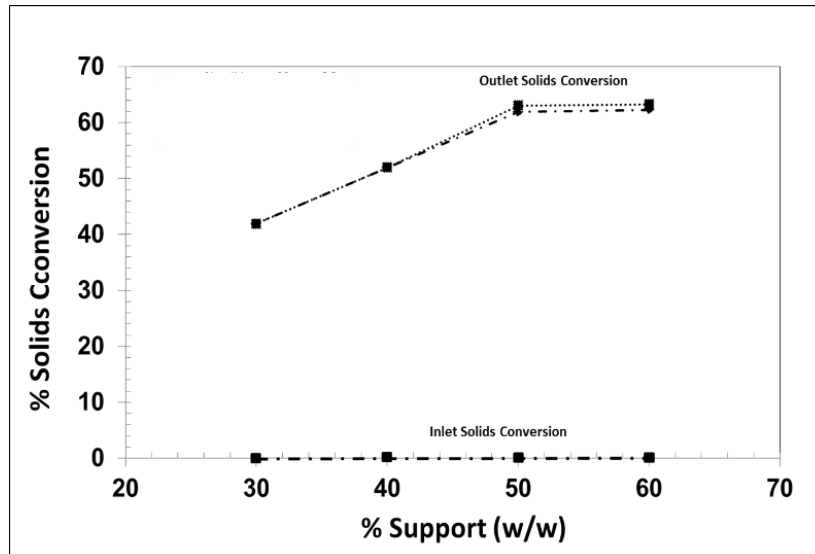

Figure 46. Comparison of reducer outlet solids conversion of varying active Fe2O3 content (high value of 70wt% Fe_2O_3 to a low value of 40wt% Fe_2O_3)
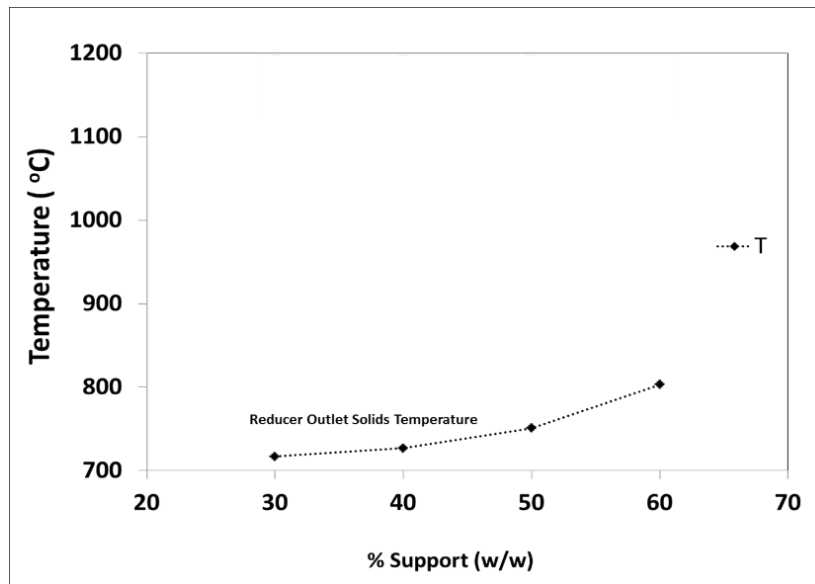

Figure 47. Comparison of reducer outlet solids temperature of varying active Fe_2O_3 content (high value of 70wt% Fe_2O_3 to a low value of 40wt% Fe_2O_3)

6.4.   Present Results to IRC and identify potential test site hosts

The technology demonstration results and the updated system analysis was reviewed with industrial partners. The demonstration results de-risked a critical technical gap associated with any chemical looping system: particle attrition. The SCL system was able to demonstrate the robustness and long-term circulation of the oxygen carrier with low particle attrition. Further, several learnings concerning on-site particle storage, handling, and transport were derisked for further commercialization efforts. The industrial committee recommended two high-level directions for evaluation, one to explore a business case for developing a larger scale SCL plant demonstration and, two to develop a broad heat integration analysis using the existing system results which provide a high degree of flexibility with a large number of sites for large-scale demonstrations. According to members of the Industrial Review Committee the installation of a new coal-based electricity or Hydrogen production plant is projected to be an active function of the ability of coal-based systems to reduce their capital costs and implementations of CO_2 emissions regulations. The modified cases with SCL for hydrogen and electricity production from coal are expected to be competitive with natural gas-based systems under a carbon-constrained scenario as per the analysis is shown in Section 7.

7. Marketing/Commercialization Discussion

The SCL system applies to new and retrofit electric and Hydrogen, carbon monoxide generating units. Currently, The United States Environmental Protection Agency (EPA) has proposed and promulgated CO_2 emission limits for new coal-fired electric utility units. Furthermore, driven by the United Nations initiative on combating climate change, a national and international surge in activity for limiting CO_2 regulations is expected to provide a robust market for the SCL system.

7.1.   Background Calculations for Marketing Plan

According to studies published by the Department of Energy[2] (DOE) pulverized coal-fired hydrogen plants are not competitive with natural gas based hydrogen generation systems. The DOE analysis (Case 2-2 for coal and Case 1-2 for natural gas) uses a consistent set of assumptions to compare competing technologies on a consistent set of technical and economic assumptions. OSU adapted the SCL

---

[2] Rath L. Assessment of hydrogen production with CO_2 capture – volume 1: baseline state-of-the-art plants. U.S. Department of Energy, DOE/NETL-2010/1434; 2010.

system to the baseline coal-based H_2 production, by assuming a mine-mouth operation which leads to an Illinois #6 coal price of \$32.93, and leads to an elimination of coal storage and transportation costs.[3] Further, co-sequestration of CO_2, SO_2 and replacement of the conventional Selexol, pressure swing adsorption and shift reactors with the SCL system allows for a reduction of 15-20% in the capital cost estimate as compared to the conventional coal system. Additionally, the use of the SCL system results in a higher power export from the combustion reaction, as opposed to the negligible power export associated with the conventional coal-based system. In addition to the technological changes resulting from SCL production, modifications to the tax code resulting from the "Furthering carbon capture, Utilization, Technology, Underground storage and reduced Emissions Act" [4] (FUTURE Act) of the 115th Congress have been examined. This act provides a credit subsidy of ~\$50/tonne for geological sequestration for any taxable year beginning in a calendar year after 2026. Applying these changes to case 2-2 in the baseline system result in a first year Hydrogen cost of \$2.2/kg. The SCL driven modifications to case 2-2 allow for a coal-SCL H_2 system to be within 10-20 cents of the required first year selling price of Hydrogen using natural gas as shown in Case 1-2. In another set of analysis, by applying SCL modifications to the case study shown in Section 6.3, allow the coal-based electricity system cost to be within \$10-15/MWh of the natural gas combined cycle (NGCC) with 90% CO_2 capture scenarios.

The cost for the SCL system is compared to the baseline system that includes a conventional water-gas shift, Selexol and pressure swing adsorption. The cost of sulfur removal in the baseline system is ~521/kW net for the capital cost portion. Replacement of this portion with a chemical looping SCL system results in a 3% reduction in the overall total plant cost. This results in an SCL system sulfur removal cost of \$495.46/kWe. The operation energy consumption for sulfur cleanup in the baseline system is ~0.041722 kWe/KWe net. The addition of chemical looping SCL system results in a 2% point increase in electrical energy efficiency and results in the operating cost reduction of sulfur control too ~0.034768kWe/kWe net. The cost estimate comparison for removal of NOx pollutant, Chlorine and mercury is equivalent to the baseline system and is <0.0007/kWe net for both the SCL system and the baseline system. The by-products for the SCL system will include sulfuric acid or gypsum depending on the specific site configuration. A full-scale SCL plant system can produce ~10 tons/hr of dilute sulfuric acid, which can be sold for ~\$30/short ton. An alternative form of sulfur by-product is Gypsum, which could be sold for \$7/ton. The potential market for by-products from the SCL technology is an attractive value addition to the overall marketing plan.

According to members of the Industrial Review Committee the installation of a new coal-based electricity or Hydrogen production plant is projected to be a strong function of the ability of coal-based systems to reduce their capital costs and implementations of CO_2 emissions regulations. The modified cases with SCL for hydrogen and electricity production from coal are expected to be competitive with natural gas based systems under a carbon-constrained scenario.

7.2.   Marketing Plan

---

[3] EIA.gov/coal April 13 to May 4, 2018. Average weekly coal commodity spot price.
[4] S.1535- 115th Congress (2017-2018): FUTURE ACT Congress.gov Library of Congress

The first step in developing a marketing plan is to demonstrate that the cost of hydrogen and electricity can be competitive under the best estimates provided under the existing economic model. The background information has shown that it is possible to make an SCL based system cost competitive. The SCL system has been demonstrated at the 250 kW$_{th}$ scale. The project results have de-risked the solids circulation and attrition rate for a 250 kW$_{th}$ fuel processing system and have provided a foundation for a 40-times scale-up in terms of fuel consumption. The specific project has demonstrated details regarding solids circulation, solids redox cycles and attrition rates that have allowed for a 10 MW$_{th}$ scale demonstration as the next relevant scale rather than 2.5 MW$_{th}$ scale. This is estimated to have reduced the commercialization time by 5-6 years. An immediate future commercialization plan includes a feasibility analysis of the system for a 10 MW$_{th}$ demonstration with Babcock and Wilcox (B&W). The commercialization pathway comprises updating the cost estimates based on additional learnings from the technology development. As a part of the commercialization plan, it was recommended by industrial review committee members to identify heat integration potential for the SCL system as different larger scale sites may have different integration requirements and utility conditions. Based on the existing operation results a broad heat integration strategy was developed.

A comprehensive energy analysis was performed to quantify the heat rates associated with the chemical looping system. This study was conducted in ASPEN Energy Analyzer and investigated in two distinct sub-cases for each case specified in Table 15. The first sub-case simulates an energy analysis that is consistent with the pilot plant demonstration at NCCC center. These set of circumstances assume that both steam and syngas are available for the chemical looping island at 400ºC. These base cases also attempt to maximize the internal heat exchanger between the various heat exchanger networks, while minimizing the utility requirements. An alternative sub-case simulation to the base case consists of situations wherein the syngas and water process streams are available at 25ºC. This offers a wide range of flexibility for potential integration into an existing or a new liquids production facility. Figure 48 and Figure 49 show the composite curve and the grand-composite curve data for Case 1 in Table 15. The heat integration strategy results show that from the composite curve and grand composite curve, the system threshold temperature indicates a high potential for high-grade heat recovery as setup in NCCC pilot plant operation. This leads to a very flexible heat exchange network configuration, that would be amenable to any site for larger scale SCL demonstration.
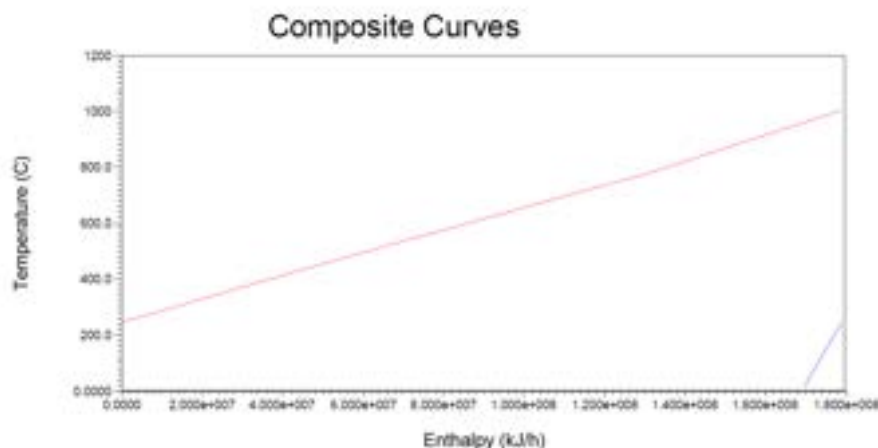
Figure 48. Composite curve for the base case associated with Case 1 in Table 2
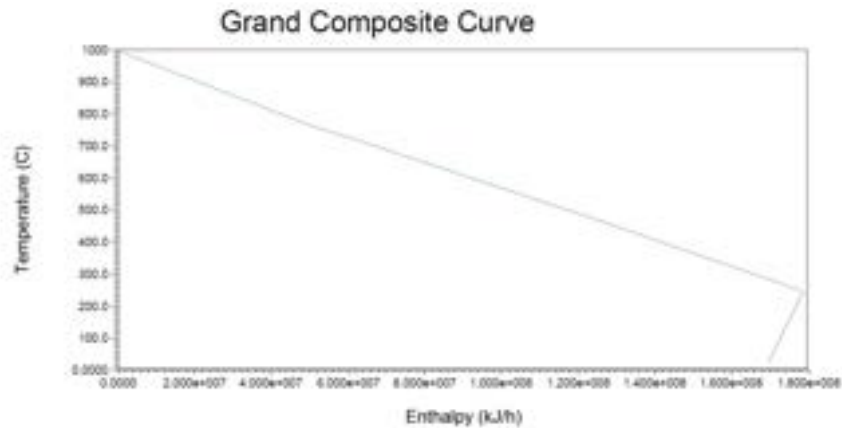

Grand Composite Curve

Figure 49. Grand composite curve for the base case associated with Case 1 in Table 2

The business case development focuses on an initial market development plan that includes specific site surveys to derisk larger scale solids circulation, manufacture of fabricated pressure vessels and evaluation of costs associated with the particular site chosen. In-state sites like the Dover power plant in Ohio and national/international sites (with the natural gas cost of ~$10/MMBTU) provided strong business case motivation for larger scale demonstration. A 10 MW$_{th}$ scale was chosen as an appropriate scale for the next scale demonstration. The team is working on identifying sites for a 10 MW$_{th}$ demonstration. This scale of operating from a technical standpoint, will derisk heat extraction schemes and hydrodynamics of large scale looping solids circulation. After identifying a site, the commercialization team plans to initiate discussions with construction companies to solicit their views on the site-specific construction pathways. The technology team plans to demonstrate a 10 MW$_{th}$ plant by 2022, a 50 MW$_{th}$ commercially relevant demonstration by 2025. The coal consumption for the 10 MW$_{th}$ plant is expected to be ~770 kg/hr and that for a 50 MW$_{th}$ commercial module demonstration is ~3850 kg/hr. CO_2